

# We are IntechOpen, the world's leading publisher of Open Access books Built by scientists, for scientists

6,000

Open access books available

148,000

International authors and editors

185M

Downloads

Our authors are among the

154

Countries delivered to

TOP 1%

most cited scientists

12.2%

Contributors from top 500 universities



WEB OF SCIENCE™

Selection of our books indexed in the Book Citation Index  
in Web of Science™ Core Collection (BKCI)

Interested in publishing with us?  
Contact [book.department@intechopen.com](mailto:book.department@intechopen.com)

Numbers displayed above are based on latest data collected.  
For more information visit [www.intechopen.com](http://www.intechopen.com)



# Multi-objective Optimisation in Abrasive Waterjet Contour Cutting of AISI 304L

*Jennifer Milaor Llanto, Ana Vafadar and Majid Tolouei-Rad*

## Abstract

The optimum waterjet machining parameters were found for maximising material removal rate and minimising surface roughness and kerf taper angle where three levels of traverse speed, abrasive flow rate, and waterjet pressure are used. The multi-linear regression equations were obtained to investigate the relationships between variables and responses, and the statistical significance of contour cutting parameters was analysed using the analysis of variance (ANOVA). Further, the response surface methodology (desirability function approach) was utilised for multi-objective optimisation. The optimum traverse speeds were 95 mm/min for 4 mm thickness and 90 mm/min for both 8 and 12 mm thicknesses. For all material thicknesses, the abrasive mass flow rate and waterjet pressure were 500 g/min and 200 MPa, respectively. The minimum values of surface roughness, kerf taper angle, and maximum material removal rate for 4-, 8- and 12-mm material thicknesses were respectively 0.799°, 1.283  $\mu\text{m}$  and 297.98  $\text{mm}^3/\text{min}$ ; 1.068°, 1.694  $\mu\text{m}$  and 514.97  $\text{mm}^3/\text{min}$ ; and 1.448°, 1.975  $\mu\text{m}$  and 667.07  $\text{mm}^3/\text{min}$ . In this study, surface roughness and kerf taper angle decreased as the waterjet pressure and abrasive mass flow rate increased; and this is showing a direct proportional relationship with traverse speed, abrasive mass flow rate and waterjet pressure.

**Keywords:** abrasive water jet, contour cutting, surface roughness, kerf taper angle, material removal rate, response surface methodology, multi-objective optimisation

## 1. Introduction

Contour cutting is one of the processes applied in metal fabrication industries. There are several non-traditional technologies employed for contour cutting, such as electro discharge machining, laser beam machining and electrochemical discharge machining, that have been noted to provide exemplary performance [1]. Accordingly, Abrasive Water Jet Machining (AWJM) is an advanced manufacturing techniques that demonstrated advantages to non-traditional machining technology owing to: its capability in cutting complex geometries, its absence of tool wear, its absence of thermal distortion, and it being environmentally friendly [2, 3]. The cutting process in AWJM is based on removing materials from a target workpiece via erosion [4]. Within this process, contour profiles in various types of programs are downloaded in a

computer-based controller, where subsequently a high-pressure pump releases pressurised water in the nozzle system. The pressurised water, moving with a high velocity, is released from the orifice in a very thin stream structure [5]. The high-speed water jet that contains abrasive particles is then accelerated to generate an abrasive waterjet. Finally, the focusing tube drives the abrasive waterjet to its target point for cutting the material [4, 6]. The compounded granular abrasive and high-pressure waterjet stream makes the abrasive waterjet capable of machining various workpieces, such as metals.

The performance of AWJM is influenced by several process parameters, which can be varied constantly within a period. In general, the primary goal of the metal fabrication industry is to manufacture high quality products in a shortened period. To attain productivity and economy objectives, it is imperative to select an optimum combination of process parameters within the abrasive waterjet cutting processes. Conventionally, the identification of the most suitable values of process parameters is accomplished by the execution of many experiments. Hence, to establish the optimum combination of process parameters in the absence of extensive experimental exertion, researchers have utilised advanced modelling techniques and optimisation in progressing the performance of abrasive waterjet cutting. For instance, Rao et al. [7] have investigated the impacts of traverse speed, standoff distance and abrasive mass flow rate in AWJM of AA631-T6. They have considered single-objective and multi-objective optimisation attributes to achieve optimum solutions by utilising Jaya and MO-Jaya algorithms, which were a posterior optimisation used to solve constrained and unconstrained conditions. The objectives of maximising material removal and minimising kerf taper angle and surface roughness were achieved by lower traverse speed and standoff distance and higher abrasive mass flow rate. Moreover, they determined that multi-objective Jaya algorithm achieved better results as compared with other algorithms, such as simulated annealing (SA), particle swarm optimization (PSO), firefly algorithm (FA), cuckoo search (CS) algorithm, blackhole (BH) algorithm, bio-geography-based optimization (BBO) algorithm, non-dominated sorting genetic algorithm (NSGA), non-dominated sorting teaching-learning-based optimization (NSTLBO) algorithm and sequential approximation optimization (SAQ). Nair and Kumanan [8] have similarly applied weighted principal components analysis (WPCA) for optimising AWJM process parameters in machining Inconel 617. These authors evaluated the impacts of abrasive mass flow rate, standoff distance, table feed and waterjet pressure against material removal rate and geometric accuracy. The WPCA method uses internal tests and training samples to calculate the 'weighted' covariance matrix, establishing that an increase in standoff distance enhances the abrasive flow volume, leading to less geometric errors and a higher rate of material removal. Equivalently, Chakraborty and Mitra [9] have applied the grey wolf optimiser (GWO) technique for AWJM cutting of AL6061 to maximise material removal rate and minimise surface roughness, simultaneously considering the constrained values of input parameters i.e., nozzle diameter and titled angle, jet feed speed, surface speed, waterjet pressure and abrasive mass flow rate. This algorithm demonstrated a faster hunting of prey (discovering the optimum parameter settings), due to the existence of a social hierarchy of grey wolves. They achieved maximum MRR via higher rate of nozzle titled angle, surface speed, waterjet pressure and abrasive mass flow rate. In the case of surface roughness, it attained its minimum value at lower rate of waterjet pressure, jet feed and surface speed and higher rate of abrasive mass flow. Trivedi et al. [10] have examined the impacts of process parameters such as pressure, traverse rate and standoff distance on surface integrity in AWJM

of AISI 316 L. Analysis of variance was employed to develop an empirical model by regression analysis for surface roughness. These authors concluded traverse speed to be the most significant parameter influencing surface roughness, whereby increasing pressure improved the surface quality of the target workpiece. Additionally, they established standoff distances, as the least contributing parameter. Research focused on optimisation of cutting operations is being continuously undertaken by researchers, where varied methods have been employed to solve different single and multi-objective optimisation problems [11–14]. Whereas single-objective optimisation problems have conventionally been applied, the performance of AWJM has mainly been measured based on multiple responses. In accordance, a multi-objective approach is required in order to optimise several categories of objective functions simultaneously. Several methods have been developed to date, and are continuously being progressed, in order to solve single-objective problems. Advances in optimisation techniques, such as: genetic algorithms (GA), simulated annealing (SA), artificial bee colony (ABC), ant colony optimization (ACO), particle swarm optimization (PSO) and teaching-learning-based optimization (TLBO), and others, have been demonstrated to be remarkably efficient in defining the optimum value of AWJM process parameters [15].

In abrasive waterjet contour-cutting, it has been realised that the impacts of most influencing factors, such as waterjet pressure, abrasive mass flow rate, standoff distance and traverse speed in straight-slit cutting, are similar with contour cutting. These research studies have shown the application of computational approaches for optimising process parameters in abrasive waterjet contour cutting requires further investigation. Therefore, this research considers the optimisation of relevant process parameters, including traverse speed, abrasive mass flow rate, and waterjet pressure on surface roughness, material removal rate and kerf taper angle in abrasive waterjet contour cutting of AISI 304L of varied thicknesses.

In this work, the experiment was designed using Taguchi orthogonal array, where a regression model has been developed to formulate the optimisation fitness function. This modelling technique has been applied to predict the response and determine optimum process parameters. In addition, response surface methodology (RSM) has been employed for multi-objective optimization, in order to obtain optimum values of input process parameters and to investigate the impacts and interactions against response parameters.

## 2. Methodology

In this study, three major steps were employed, consisting of abrasive waterjet contour cutting experiments, regression modelling and optimisation. The experiment, modelling and optimisation procedures are presented in **Figure 1**. The experiment was conducted using the Taguchi L<sub>9</sub> orthogonal array to analyse the impacts of input parameters, i.e., traverse speed, abrasive mass flow rate and waterjet pressure. Desirability analysis using response surface methodology is employed for the experimental results of material AISI 304L. In this desirability analysis, multi-responses are considered. It establishes the optimum set of the selected process parameters on the performance characteristics.

A regression model was developed using the machining process parameters from the experimental execution to extract mathematical models. A linear stepwise regression analysis was performed to predict the surface roughness, material removal rate

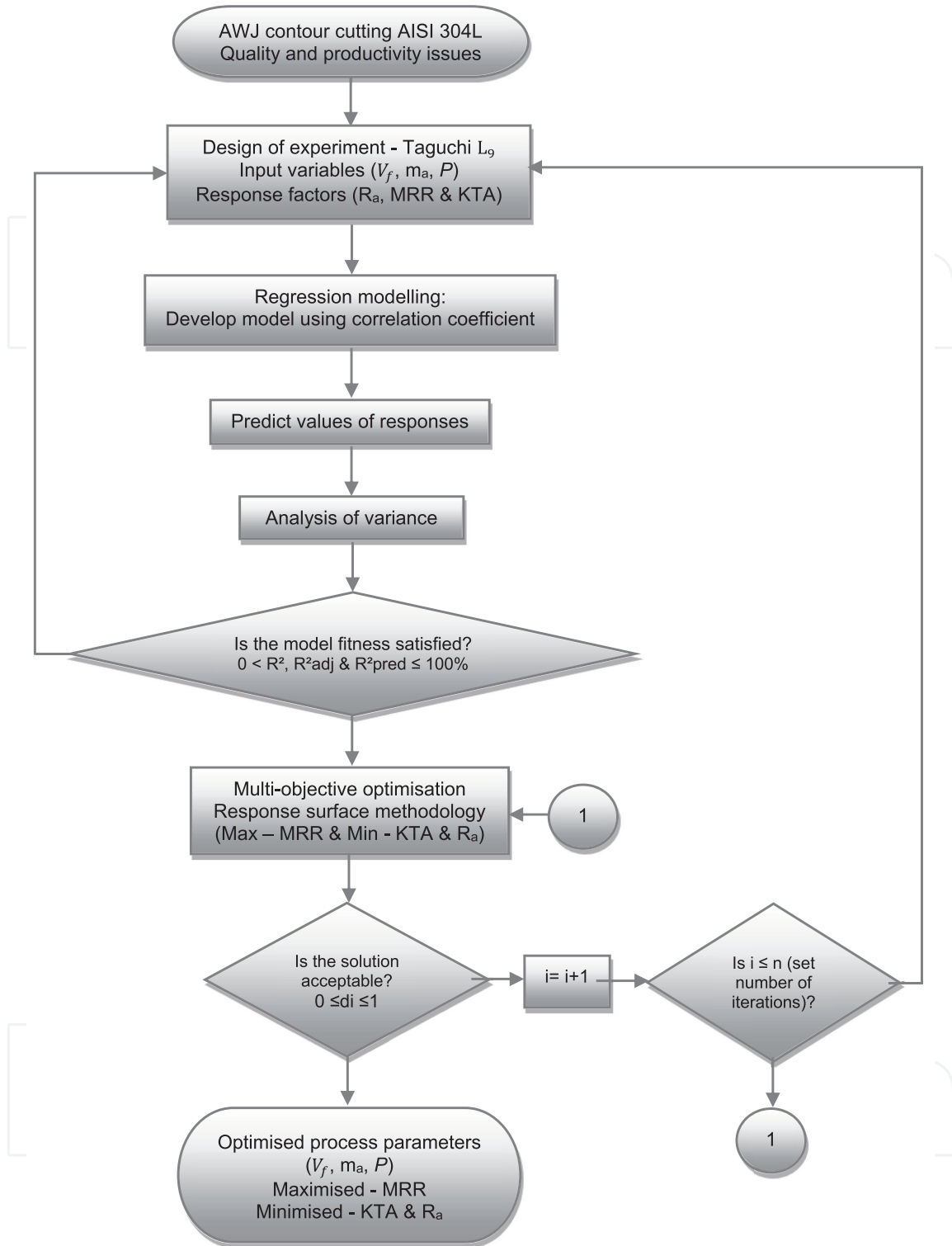


**Figure 1.**  
Multi-objective optimisation process flow chart.

and kerf taper angle value. The reliability of the models generated was assessed based on coefficient of determination ( $R^2$ ,  $R^2_{adj}$  &  $R^2_{pred}$ ). However, supposing that regression models are not within the acceptable range or do not provide preferable values of coefficients of determination set by the decision-maker, it is anticipated that these models will not provide precise prediction. Therefore, the selected parameter setting conflicts with the response variables, denoting the necessity for modification of independent variables or experimental design [16].

Referring to **Figure 1**, after achieving the fittest models, a multi-objective optimisation was performed by using response surface methodology with the objectives of maximising material removal, whilst minimising surface roughness and kerf taper angle. The number of solutions and iterations ( $i = 1$  to  $n$ ) may vary, depending on the machining process requirements to establish the best alternative or solution. Hence, if the composite desirability is not within the tolerable array, several iterations repeating the response surface optimisation were executed. Subsequently, if these repetitions reached the maximum number of iterations and the composite desirability is not attaining adequate values, modifying the design of experiments and the corresponding independent variables or its values is necessary [16]. Moreover, in some cases, other soft computing techniques should be considered [17].

## 2.1 Material and experimental design

In this work, the material machined in the experiments was AISI 304L with varied thicknesses of 4, 8 and 12 mm. The assigned material thicknesses with differing uniform gaps were used to gain a better yield of variations in AWJM cutting behaviour. Stainless steel, such as AISI 304L, is widely used in fabrication industries, where it is recognised for its high strength and corrosion and heat resistance. This results from its high alloying content of Cr and Ni [18]. The chemical and mechanical composition of this material is detailed in **Table 1**.

The setup consisted of an OMAX MAXIEM 1515 abrasive waterjet machine, possessing a direct drive pump and dynamic cutting head with maximum pressure of 413.7 MPa and cutting area of 2235 mm length and 1727 mm width. The cutting head is comprised of a mixing chamber for abrasive and waterjet, along with a nozzle diameter of 0.56 mm and a jet impact angle of 90°. An abrasive garnet with a mesh size of #80 was utilised for abrasive waterjet cutting experiments. The unit is inclusive of IntelliMax software, where the experiment setup conditions were uploaded and entered. The cutting head can move in the Z-axis over a distance of 305 mm, with a maximum traverse speed of 12,700 mm/min. Standoff distance was designated to 1.5 mm in agreement with recommended range for abrasive waterjet machining in previous works [20, 21]. The AWJM setup and process parameters are demonstrated in **Figure 2**.

Chemical composition in wt.%		Mechanical properties	
C	0.03	Hardness, Rockwell B	82
Mn	2	Tensile Strength, Ultimate, MPa	564
Si	0.75	Tensile Strength, Yield, MPa	210
Cr	18.00–20.00	Elongation at Break	58%
Ni	8.00–12.00	Modulus of Elasticity, GPa	193–200
P	0.045		
S	0.03		
Ni	0.1		
Fe	Remaining		

**Table 1.**  
 Chemical and mechanical composition of AISI 304L [19].

Upon completion of the experiments, the roughness of the machined surfaces was quantified by a surface roughness tester (TR200 model). **Figure 2** presents the cut surface captured by LEICA M80, which indicates the measurement area for the roughness. The kerf top and bottom width were measured using a LEICA M80 optical microscope model. Moreover, rate of material removal and kerf taper angle were calculated using Eqs. (1) and (2), respectively [11]. The roughness of the cut surface determined according to the ISO/TC 44 N 1770 standard, ( $\mu\text{m}$ );  $W_t$  is width of the cut surface at the jet inlet, (mm);  $W_b$  is the width of the cut surface at the jet outlet, (mm);  $u$  is the angularity or perpendicular deviation, (mm);  $\alpha^\circ$ - inclination angle of the cut surface, ( $^\circ$ ); MRR is the Material Removal Rate, ( $\text{mm}^3/\text{min}$ );  $t$  is the thickness of the material (mm) [22].

$$MRR = ht \left( \frac{W_t + W_b}{2} \right) V_f \quad (1)$$

$$KTA = \text{Arctan} \left( \frac{W_t + W_b}{2ht} \right) \quad (2)$$

The input parameters considered in abrasive waterjet contour cutting in this experiment included traverse rate ( $V_f$ ), abrasive flow rate ( $m_a$ ) and water pressure ( $P$ ), as these parameters have been demonstrated in previous studies as having significant impacts in AWJM applications [10, 12, 23, 24]. Surface integrity, kerf geometries

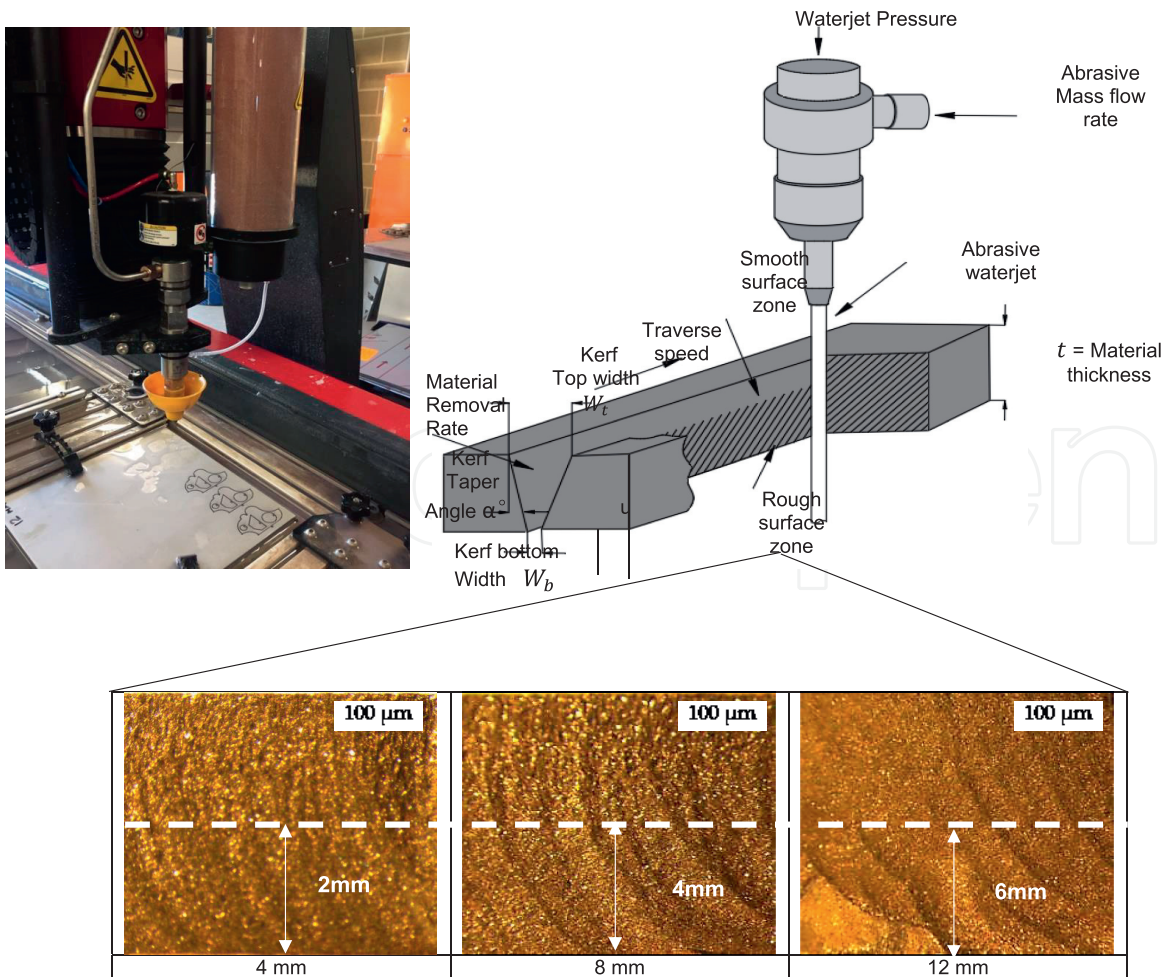


**Figure 2.**  
AWJM setup and process parameters.

and low material removal rate evidence has been reported in machining of AISI 304L, requiring further improvement [4, 25]. Furthermore, taper angles formed in AWJM demonstrate different inclinations as contour curvature radius differs [26]. Hence, quality and productivity are an intensified demand in various manufacturing fields and are significant performance indicators for machining processes. Therefore, in this study, material removal rates (MRR), surface roughness ( $R_a$ ) and kerf taper angle (KTA) have been chosen as process parameter characteristics for abrasive waterjet contour cutting investigations, due to their influence against the selected input parameters. The levels of the considered independent variables, responses and coding assignment have been detailed in **Tables 2** and **3**.

Abrasive waterjet cutting was executed for three different profiles, representing straight-line, inner arcs and outer arcs, as part of the completed twelve profiles, as demonstrated in **Figure 2**. The abovementioned profiles were selected to confirm a broad array of complicated machining profiling applications. The levels of profiles employed showed occurrences of surface roughness, low machining rate and inaccuracies of cut geometries in regard to previous works [27, 28], recommending further studies, predominantly for difficult-to-cut materials, such as AISI 304L (**Figure 3**).

The design of experimentation (DOE) was carried out using the Taguchi approach in MINITAB 19 software. The Taguchi method is useful in determining the best combination of factors under desired experimental conditions, reducing the large number of experiments which would be required in traditional experiments as the number of process parameter increases [29, 30].

In Taguchi's approach, selection of the appropriate orthogonal array depends on aspects such as: the number of input and response factors along with the interactions that are of key significance; number of levels of data for input factors; and required resolution of experiment and limitations cited on cost and performance [29, 31]. With this specific advantage, this method is suitable in conducting experiments with an appropriate number of tests to determine the optimal combination and significance of the selected factors [32]. The relevant variation in thicknesses dictates different material responses. Therefore, Taguchi  $L_9$  orthogonal array was executed for three

Independent variables	Codes	Levels		
		1	2	3
Traverse speed, $V_f = \text{mm/min}$	$X_1$	90	120	150
Abrasive mass flow rate, $m_a = \text{g/min}$	$X_2$	300	400	500
Waterjet pressure, $P = \text{MPa}$	$X_3$	200	250	300

**Table 2.**  
 Levels of input process parameters.

Profiles	Surface roughness, $\mu\text{m}$	Material removal rate, $\text{mm}^3/\text{min}$	Kerf taper angle, $^\circ$
Straight-line, 20 mm	$R_{a1}$	MRR1	KTA1
Inner arc, R10	$R_{a2}$	MRR2	KTA2
Outer arc, R20	$R_{a3}$	MRR3	KTA3

**Table 3.**  
 Output parameters for varied profiles.



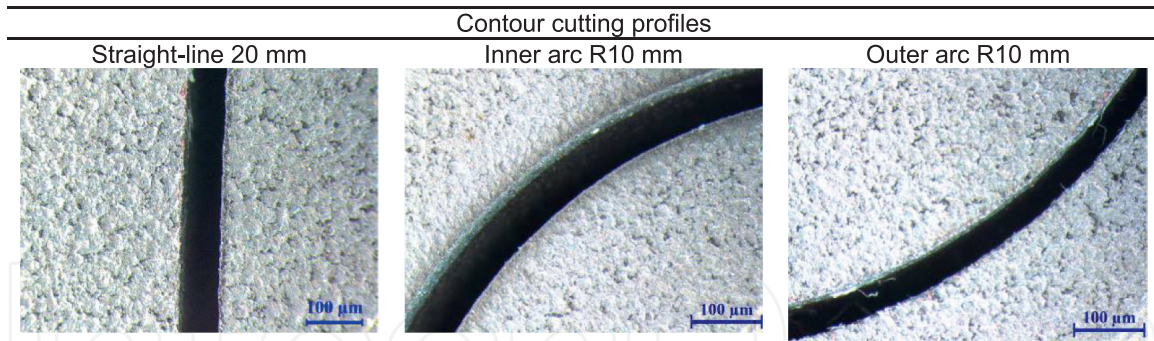


**Figure 3.**  
Abrasive waterjet contour cutting profiles.

Exp. No.	Input Parameters		
	$V_f$ (mm/min)	$m_a$ (g/min)	$P$ (MPa)
1	90	300	200
2	90	400	250
3	90	500	300
4	120	300	250
5	120	400	300
6	120	500	200
7	150	300	300
8	150	400	200
9	150	500	250

**Table 4.**  
Taguchi  $L_9$  orthogonal array.

levels of material thicknesses ( $t$ ), i.e., 4, 8 and 12 mm, as presented in **Table 4**. The AWJM performances were analysed accordingly by the applied material thickness.

## 2.2 Modelling and multi-objective optimisation

A mathematical model was developed to associate the input process parameters to the response's characteristics. To achieve this, a linear regression was employed to develop models for the prediction of responses. The empirical model for the prediction of the responses in regard to controlling parameters was established by linear regression analysis. Regression analysis was then applied to obtain the interactions between independent and dependent variables [33]. Multi-linear regression involves regression analysis of dependent and independent variables exhibiting a linear relationship [34]. It stipulates the relationship between two or more variables and a response variable by fitting a linear equation to examine data. The value of the independent variable  $x$  or process parameter is correlated with a value of the dependent variable,  $y$ , which is the output parameter. In general, this analysis is applied to investigate the degree of relationship between multiple variables fitted by a straight line [33].

In general, regression model is expressed by Eq. (3) [33].

$$y = \alpha + \beta_1 x_1 + e \quad (3)$$

$$\text{Wherein : } e = y_1 - \hat{y}_1 \quad (4)$$

where,  $y$  = dependent variable,  $\alpha$  = constant,  $x_1$  = Independent variable,  $\beta_1$  = coefficient of independent variable  $x_1$ ,  $e$  = error,  $y_1$  = regression line values and  $\hat{y}_1$  = actual observation.

If this involves more than one variables, then it is categorised as multi-regression as shown in Eq. (5) [33].

$$y = \alpha + \beta_1 x_1 + \beta_2 x_2 + \beta_3 x_3 + \dots \dots \dots \beta_n x_n + e_n \quad (5)$$

A multi-linear regression analysis can be employed to fit a predictive model to an observed data set of values of output and input variables. The obtained results of surface roughness, material removal rate and kerf taper angle were expressed in terms of the input parameters such as traverse speed ( $X_1$ ) abrasive mass flow rate ( $X_2$ ) and waterjet pressure ( $X_3$ ).

The predicted values are functional for optimising the parameters by providing an adequate comprehension of the significant parameters. The percentage of error between the experimental data and acquired predicted values has been calculated based on Eq. (6) [33]. The relative percentage of error was acceptable at <20% [35].

$$\text{Error} = \frac{1}{n} \sum_n \left[ \frac{\text{Response}_{(\text{experiment})} - \text{Response}_{(\text{predicted})}}{\text{Response}_{(\text{experiment})}} \right] \% \quad (6)$$

The performance of the established regression model was assessed by statistical approaches to confirm the goodness-of-fit of the model and the impact of the predicted variables. Following this, the significance and effectiveness of the developed models were validated by *analysis of variance*. *Analysis of variance (ANOVA)* is a statistical method that facilitates the evaluation of comparative influences for each control parameter [36, 37]. The significance of input parameters including traverse speed, abrasive mass flow rate and waterjet pressure were investigated using  $p$ - values and determination of coefficient ( $R^2$ ). In this work, a confidence interval of 95% ( $p < 0.05$ ) has been applied that is in alignment with previous works [29, 38, 39]. A 95% confidence interval means that there is only a 5% chance of being the wrong estimation; therefore, the influence of each process parameter or other interactions on the responses is considered insignificant if their  $p$ -values were estimated at more than 0.05 [37].

The determination of coefficient ( $R^2$ ,  $R^2_{\text{adj}}$  and  $R^2_{\text{pred}}$ ) refers to the percentage variation of responses ranging from 0–100%. These indicators determine the adequacy of the model against obtained experimental data and predicted observation. This  $R^2$ ,  $R^2_{\text{adj}}$  and  $R^2_{\text{pred}}$  value of  $\geq 80\%$ , proved a better model fits of the obtained data [35].

Response surface methodology (RSM) can be utilised for multi-objective optimisation. This multi-desirability is based on multi-response optimisation using an objective function  $D(X)$ , denoted as desirability function [40]. This method translates each response ( $y_i$ ) into a desirability function ( $d_i$ ), differing in the array of  $0 \leq d_i \leq 1$ ,

where desirability function =0 indicates an undesirable response and desirability function =1 represents a fully desired response [41]. The objective function D is specified by Eq. (7) [40].

$$D = (d_1 \times d_2 \times \dots \times d_n)^{1/n} = \left( \prod_{i=1}^n d_i \right)^{1/n} \quad (7)$$

The effectiveness of multi-objective optimisation is anticipated based on the method used for establishing priority weights for each response characteristics [42]. Generally, equal importance is set for selected responses; hence, weights may differ depending on the machining process requirements in order to establish the most suitable solution [43].

A simultaneous optimisation process was employed to determine the levels of resulting to the maximum overall desirability. The responses namely  $R_a$ , MRR and KTA were optimised concurrently to assess the set of input process parameters with the objectives of maximising MRR and minimising  $R_a$  and KTA.

### 3. Results and discussion

#### 3.1 Regression models and analysis for surface roughness

The multi-linear regression coefficients are summarised in **Table 5**, exhibiting the correlation between the input parameters and the output surface roughness for straight-line, inner and outer arc profiles for material thicknesses of 4, 8 and 12 mm. The values of coefficients for all profiles and thicknesses demonstrate a similar trend, showing that constant and variable  $X_1$  is positive and variables  $X_2$  and  $X_3$  are negative. The coefficient indicates the change in the mean response relating in the variation of the specific term, whilst the other term in the model remains constant. The relationship between a term and response is denoted by the sign of the coefficient [44]. The negative correlation coefficient denotes an inverse relationship between variables and responses; and therefore, if it is positive as the coefficient increases, the response mean value also increases. Therefore, an increasing rate of traverse speed ( $X_1$ ) results in an incremental value of surface roughness. Moreover, an increasing rate of abrasive mass flow and waterjet pressure indicates/obtains a decreasing value of surface roughness. The values of  $R^2$ ,  $R^2_{adj}$  and  $R^2_{pred}$  for 4, 8 and 12 mm ranged from 94.33–99.08%, 90.94–98.52% and 88.66–96.17%, respectively. This indicates that regression models denote an acceptable confirmation of the relationship between the independent variables and  $R_a$  response, which denotes a high significance of the model. Therefore, the multi-linear model is reliable and can be utilised in the optimisation of process parameters. It can be observed that the  $R^2$ ,  $R^2_{adj}$  and  $R^2_{pred}$  obtained from straight-line, inner and outer arcs profiles have a uniform gap of at least 2%, which is comparable for all material thicknesses. Hence, this minimal gap denotes an insignificant difference between the surface roughness achieved from straight and curvature profiles [36].

The results detailed in **Table 5** show that the highest value of  $R^2$ ,  $R^2_{adj}$  and  $R^2_{pred}$  for 4 and 8 mm material thickness are achieved in  $R_{a3}$  with the values of 97.26, 94.84 and 92.45%; 98.64, 97.82 and 95.06%; 99.08, 98.52 and 96.17% respectively. Thus,  $R_{a2}$  achieved the highest percentage of  $R^2$ ,  $R^2_{adj}$  and  $R^2_{pred}$  for 12 mm material thickness

Term	<i>t</i> = 4 mm			<i>t</i> = 8 mm			<i>t</i> = 12 mm		
	R <sub>a1</sub>	R <sub>a2</sub>	R <sub>a3</sub>	R <sub>a1</sub>	R <sub>a2</sub>	R <sub>a3</sub>	R <sub>a1</sub>	R <sub>a2</sub>	R <sub>a3</sub>
	Coef	Coef	Coef	Coef	Coef	Coef	Coef	Coef	Coef
	1.418	1.5394	1.4256	2.097	1.8107	1.76	2.542	2.3854	2.272
$\beta_1$	0.003522	0.002944	0.003222	0.009814	0.003483	0.008869	0.005389	0.004276	0.003090
$\beta_2$	- 0.000310	- 0.000300	- 0.000217	- 0.001464	- 0.000422	- 0.000577	- 0.000450	- 0.000446	- 0.000515
$\beta_3$	- 0.001500	- 0.001300	- 0.001133	- 0.001955	- 0.000977	- 0.001920	- 0.002567	- 0.001924	- 0.001081
Model Summary									
R <sup>2</sup>	95.26%	96.77%	97.26%	98.01%	98.16%	98.64%	97.73%	99.08%	94.33%
R <sup>2</sup> (adj)	92.41%	92.41%	94.84%	96.82%	97.05%	97.82%	96.37%	98.52%	90.94%
R <sup>2</sup> (pred)	90.58%	90.58%	92.45%	93.84%	93.77%	95.06%	93.33%	96.17%	88.66%

**Table 5.**  
Summary of multi-linear regression coefficients for R<sub>a</sub>.

with the values of 99.08%, 98.52% and 96.17% accordingly. Therefore, the most fitted and predominant models were  $R_{a3}$  for both 4 and 8 mm, and  $R_{a2}$  for 12 mm material thickness. The predicted  $R_a$  values of regression models applied for straight-line, inner and outer arcs profiles of three levels of material thicknesses are detailed in **Tables 6-8**. The percentage error obtained for 4, 8 and 12 mm AISI 304L thicknesses ranged from  $-4.22$  to  $3.44\%$ ,  $3.30$  to  $6.71\%$  and  $-5.75$  to  $2.49\%$ , respectively. The errors determined for  $R_a$  between the predicted value and experimental results are less than 20%, denoting that these models are reliable for predicting  $R_a$  values.

**Figure 4** presents the residual plot for  $R_a$ , consisting of normal probability plot, residual versus fits, histogram for residuals and residuals versus experimental values for the most fitted regression models for 4, 8 and 12 mm, at  $R_{a3}$ ,  $R_{a3}$  and  $R_{a2}$ , respectively. Similarly, the normal probability plots for all the material thicknesses demonstrated a close fit to a line in a normal probability graph. The points forming an

Exp. no.	Independent variables			$R_{a1}$ ( $\mu\text{m}$ )			$R_{a2}$ ( $\mu\text{m}$ )			$R_{a3}$ ( $\mu\text{m}$ )		
	$X_1$	$X_2$	$X_3$	Exp.	Pred.	Error %	Exp.	Pred.	Error %	Exp.	Pred.	Error %
1	90	300	200	1.35	1.34	0.81	1.43	1.42	0.61	1.46	1.45	0.56
2	90	400	250	1.25	1.24	1.41	1.33	1.35	-1.56	1.37	1.36	1.06
3	90	500	300	1.09	1.13	-3.99	1.25	1.27	-1.72	1.24	1.26	-2.44
4	120	300	250	1.36	1.37	-1.26	1.46	1.46	-0.39	1.48	1.48	0.22
5	120	400	300	1.29	1.27	2.35	1.42	1.39	3.44	1.40	1.38	1.72
6	120	500	200	1.41	1.39	2.45	1.50	1.48	2.28	1.48	1.48	-0.28
7	150	300	300	1.41	1.40	0.68	1.50	1.50	-0.39	1.49	1.50	-1.11
8	150	400	200	1.48	1.52	-4.22	1.58	1.60	-1.56	1.58	1.60	-2.11
9	150	500	250	1.43	1.42	1.77	1.51	1.52	-0.72	1.53	1.51	2.39

**Table 6.**  
Predicted  $R_a$  values of regression models for  $t = 4$  mm.

Exp. no.	Independent variables			$R_{a1}$ ( $\mu\text{m}$ )			$R_{a2}$ ( $\mu\text{m}$ )			$R_{a3}$ ( $\mu\text{m}$ )		
	$X_1$	$X_2$	$X_3$	Exp.	Pred.	Error %	Exp.	Pred.	Error %	Exp.	Pred.	Error %
1	90	300	200	2.12	2.15	-3.30	1.81	1.80	1.06	2.01	2.00	0.47
2	90	400	250	1.88	1.91	-2.73	1.72	1.71	0.86	1.86	1.85	0.98
3	90	500	300	1.64	1.66	-2.16	1.60	1.62	-2.04	1.65	1.69	-4.40
4	120	300	250	2.41	2.35	6.71	1.84	1.86	-1.81	2.16	2.17	-1.14
5	120	400	300	2.14	2.10	3.38	1.78	1.77	1.29	2.08	2.02	6.23
6	120	500	200	2.22	2.15	6.30	1.83	1.82	0.74	2.16	2.15	0.79
7	150	300	300	2.52	2.54	-1.89	1.92	1.91	0.63	2.32	2.34	-2.15
8	150	400	200	2.56	2.59	-3.68	1.95	1.97	-1.92	2.46	2.48	-1.58
9	150	500	250	2.32	2.35	-2.62	1.89	1.88	1.18	2.33	2.32	0.79

**Table 7.**  
Predicted  $R_a$  values of regression models for  $t = 8$  mm.

Exp. no.	Independent variables			R <sub>a1</sub> (μm)			R <sub>a2</sub> (μm)			R <sub>a3</sub> (μm)		
	X <sub>1</sub>	X <sub>2</sub>	X <sub>3</sub>	Exp.	Pred.	Error %	Exp.	Pred.	Error %	Exp.	Pred.	Error %
1	90	300	200	2.39	2.38	1.17	2.26	2.25	0.42	2.18	2.18	-0.09
2	90	400	250	2.20	2.21	-0.50	2.12	2.11	0.60	2.09	2.07	1.20
3	90	500	300	2.00	2.03	-3.17	1.95	1.97	-1.98	1.99	1.97	2.49
4	120	300	250	2.42	2.41	0.83	2.29	2.28	0.30	2.22	2.22	0.69
5	120	400	300	2.25	2.24	1.17	2.16	2.14	2.03	2.05	2.11	-5.75
6	120	500	200	2.48	2.45	3.00	2.29	2.29	-0.39	2.15	2.17	-2.15
7	150	300	300	2.45	2.45	0.50	2.30	2.32	-1.36	2.27	2.26	1.46
8	150	400	200	2.60	2.66	-5.67	2.45	2.46	-1.34	2.32	2.31	0.43
9	150	500	250	2.51	2.48	2.67	2.34	2.32	1.74	2.22	2.21	1.72

**Table 8.**  
 Predicted R<sub>a</sub> values of regression models for t = 12 mm.

approximately straight-line and falling along the fitted line denotes that the data is normally distributed and there is a good relation between measured and estimated response values [45]. In general, the residuals versus fits and observation graph for each material thickness display that the points are distributed randomly and near both sides of 0, with no distinguished pattern denoting a minimal deviation within residuals and estimated values. This graph plots the difference between the experimental data as predicted on the y-axis and the fitted or predicted values on the x-axis, to validate the assumption that the residuals have constant variance [46].

**Figure 4** also exhibits the histogram graph for R<sub>a</sub>, illustrating the distribution or frequency of the residuals for all observations. The data shows the frequency of R<sub>a</sub> for 4, 8 and 12 mm material thicknesses to range from -0.02 to 0.03, -0.05 to 0.05 and -0.02 to 0.02, respectively. The histogram presents distribution of the surface roughness obtained from varying material thicknesses. **Figure 4** histogram of residuals denotes that the residuals are normally distributed. These results reveal a minimal interval of inequalities of the experimental data, indicating that the R<sub>a</sub> models meet their assumptions and are well fitted for the accuracy of prediction [46]. The effects of process parameters were established by ANOVA, where surface roughness results are given in **Tables A1-A3** in the Appendix section.

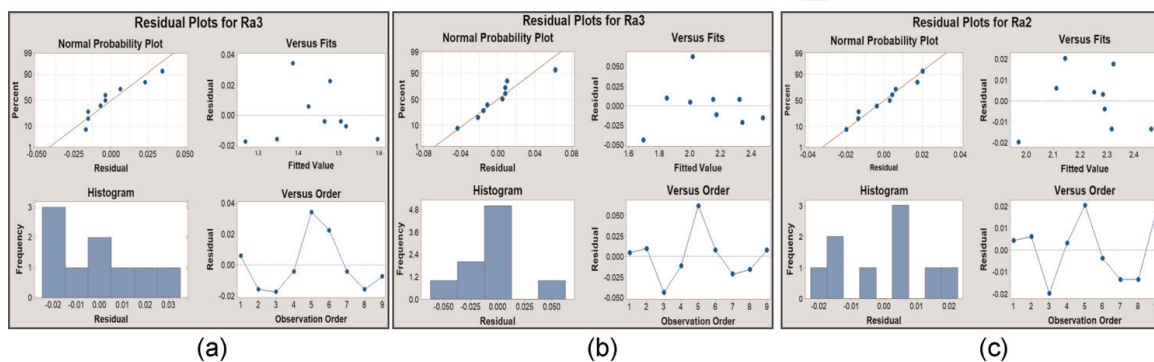


**Figure 4.**  
 Residual plots for surface roughness. (a) R<sub>a3</sub> (μm) for t = 4 mm (b) R<sub>a3</sub> (μm) for t = 8 mm (c) R<sub>a2</sub> (μm) for t = 12 mm.

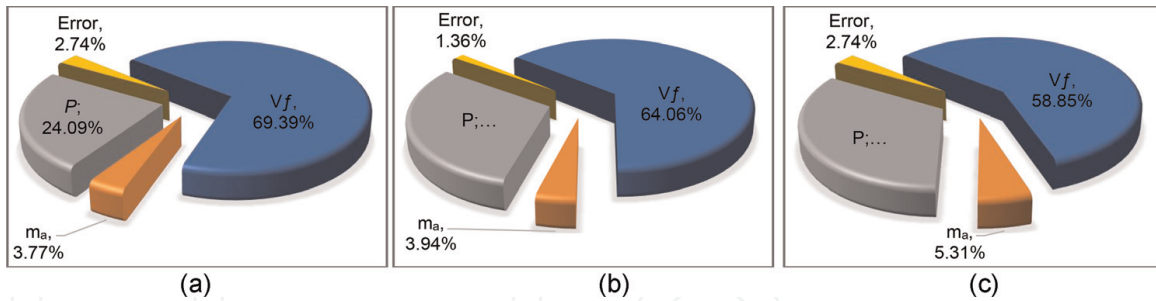


**Figure 5.** Percentage contribution of variables for surface roughness. (a)  $R_{a3}$  ( $\mu\text{m}$ ) for  $t = 4$  mm (b)  $R_{a3}$  ( $\mu\text{m}$ ) for  $t = 8$  mm (c)  $R_{a2}$  ( $\mu\text{m}$ ) for  $t = 12$  mm.

The impacts of the parameters for all profiles across the three levels of material thicknesses demonstrated a similar trend, denoting traverse speed and waterjet pressure to be significant factors for acquiring p-Values lower than 0.05, as detailed in **Tables A1-A3**. Accordingly, this work has established that abrasive mass flow rate is an insignificant input parameter for obtaining p-Values  $>0.05$ , ranging from 0.002 to 0.067. **Figure 5** represents the percentage contribution of variables for  $R_a$  of the most fitted regression models for 4, 8 and 12 mm material thickness. Overall, traverse speed features as the most influencing parameter, followed by waterjet pressure and abrasive mass flow rate. It can be observed here that the influence of traverse speed decreases, ranging from 69.39 to 58.85%, as the material thickness increases. In AWJM, an increasing traverse speed reduces the number of abrasive particles, leading to higher occurrences of surface roughness [47]. **Figure 5** shows that as the material thickness increases, the percentage contribution of waterjet pressure and abrasive mass flow rate also increases, ranging from 24.09 to 33.1% and 3.77 to 5.31%, respectively. The increasing value of waterjet pressure denotes higher energy, reinforcing a larger amount of abrasive particles obtaining lower surface roughness [48]. Further, an increasing rate of abrasive mass flow breaks down abrasive particles into smaller sizes, resulting in more sharp edges that reduce surface roughness [15]. The percentage errors obtained were less than 20%, indicating acceptable reliability of the models, as described in Eq. (6).

### 3.2 Regression model and analysis for material removal rate

**Table 9** displays multi-linear regression coefficients of models developed for material removal rate against input parameters i.e., traverse speed ( $X_1$ ), abrasive mass flow rate ( $X_2$ ) and waterjet pressure ( $X_3$ ) for 4, 8 and 12 mm material thicknesses of AISI 304L. Regardless of material thickness and cutting profile category, the input parameter coefficients acquired a positive sign whilst the constant coefficients had a negative sign. The sign of the coefficient denotes the trend of relationship between variables and response [44]. As a result, an increasing rate of traverse speed, abrasive mass flow rate and waterjet pressure, generates a higher rate of material removal. Overall, the coefficient of determination  $R^2$  ranged from 97.79 to 97.92%, with  $R^2_{\text{adj}}$  ranging from 96.46 to 96.67% and  $R^2_{\text{pred}}$  ranging from 92.53 to 94.35%, confirming that all generated regression models were significant. The models were established to be sufficient for accurate forecasting of material removal rate within the assigned levels of input parameters for AWJM of straight and arcs profiles. Furthermore, **Table 9** demonstrated that MRR1 (straight-line), MRR2 (inner

Term	$t = 4 \text{ mm}$			$t = 8 \text{ mm}$			$t = 12 \text{ mm}$		
	MRR1	MRR2	MRR3	MRR1	MRR2	MRR3	MRR1	MRR2	MRR3
	Coef	Coef	Coef	Coef	Coef	Coef	Coef	Coef	Coef
	-84.2	-33	-22.8	-119	-45	-60.6	-158.8	-43.3	-73.5
$\beta_1$	1.752	1.562	1.440	2.941	2.658	2.708	3.867	4.476	3.416
$\beta_2$	0.1260	0.0833	0.0901	0.2723	0.1738	0.0333	0.3960	0.205	0.2437
$\beta_3$	0.5103	0.3430	0.4101	0.7770	0.775	0.950	0.917	0.511	1.080
Model Summary									
$R^2$	97.92%	97.56%	97.54%	98.86%	97.71%	94.73%	98.70%	96.37%	97.79%
$R^2$ (adj)	96.67%	96.09%	96.06%	98.18%	96.33%	91.56%	97.92%	94.20%	96.46%
$R^2$ (pred)	94.35%	90.74%	91.12%	95.73%	91.90%	82.30%	95.19%	89.41%	92.53%

**Table 9.**  
 Summary of linear regression coefficients for MRR.

arcs) and MRR3 (outer arcs) attained a uniform gap of at least 2% for  $R^2$ ,  $R^2$ adj and  $R^2$ pred values. This nominal disparity of the coefficient of determination indicates that AWJM performance for straight and curvature profiles are not significantly different from one another [36]. The results detailed in **Table 9** confirm that the highest values of  $R^2$ ,  $R^2$ adj and  $R^2$ pred for all material thicknesses was attained in MRR1 (straight-line profile) with values of 97.92, 96.67 and 94.35%; 98.86, 98.18 and 95.73%; 98.70, 97.92 and 95.19% respectively. This statistical measurement evaluates the relationship between the model and response variables, indicating that a value nearest to 100% denotes a more reliable model [49]. Therefore, MRR1 regression models are considered as the most fitted model for 4, 8 and 12 mm material thicknesses.

**Tables 10-12** present the predicted MRR values using the generated regression models of 4, 8 and 12 mm thickness of AISI 304L for three varied contour profiles. The percentage error acquired for 4, 8 and 12 mm AISI 304L thicknesses ranged from -5.35 to 5.15%, -6.59 to 4.77% and -5.05 to 6.62%, respectively. The errors determined for  $R_a$  between the predicted value and experimental results were less than 20%, indicating models to be well fitted for predicting MRR values.

Plots of all residuals of the best material removal rate (MRR1) for all material thicknesses are represented in **Figure 6**. Overall, the normal probability plots for all the material thicknesses illustrate that the adjacency of the points are linear indicating there is no deviation from the assumptions, because they are normally and independently distributed [46]. Residuals versus fits and observation for MRR1 of straight-line, inner and outer arc profiles confirm that there is no skewness or outlier pattern, revealing that individual deviated assumptions have no conflicts or contradictions. **Figure 6** also presents the histogram graph for MRR1, obtaining frequency ranging from -10 to 15 for 4 mm, -15 to 15 for 8 mm and -18 to 20 for 12 mm material thicknesses. These results signify that the distribution or frequency of residuals for all observations fell in minimal interval or inequalities of the experimental data, justifying the adequacy of the suggested MRR1 models [46].

According to the results presented in **Tables A4-A6** in the Appendix section, detailing ANOVA for material removal rate, the effects of the input parameters for



Exp. no.	Independent variables			MRR 1 (mm <sup>3</sup> /min)			MRR 2 (mm <sup>3</sup> /min)			MRR 3 (mm <sup>3</sup> /min)		
	X <sub>1</sub>	X <sub>2</sub>	X <sub>3</sub>	Exp.	Pred.	Error %	Exp.	Pred.	Error %	Exp.	Pred.	Error %
1	90	300	200	216.2	213.3	1.36	212.1	201.2	5.15	217.7	215.9	0.83
2	90	400	250	248.6	251.4	-1.10	223.1	226.7	-1.60	242.4	245.5	-1.27
3	90	500	300	284.2	289.5	-1.86	250.6	252.1	-0.62	267.8	275.0	-2.68
4	120	300	250	280.6	291.3	-3.82	251.7	265.2	-5.35	283.0	279.6	1.19
5	120	400	300	342.5	329.4	3.82	293.7	290.7	1.03	313.7	309.2	1.44
6	120	500	200	298.8	291.0	2.61	263.5	264.7	-0.45	286.2	277.2	3.14
7	150	300	300	372.1	369.4	0.73	333.8	329.2	1.38	343.9	343.4	0.16
8	150	400	200	330.7	330.9	-0.07	299.6	303.2	-1.21	298.5	311.4	-4.32
9	150	500	250	361.5	369.1	-2.09	333.5	328.7	1.44	344.8	340.9	1.14

**Table 10.**  
Predicted MRR values of regression model for t = 4 mm.

Exp. no.	Independent variables			MRR 1 (mm <sup>3</sup> /min)			MRR 2 (mm <sup>3</sup> /min)			MRR 3 (mm <sup>3</sup> /min)		
	X <sub>1</sub>	X <sub>2</sub>	X <sub>3</sub>	Exp.	Pred.	Error %	Exp.	Pred.	Error %	Exp.	Pred.	Error %
1	90	300	200	367.9	382.8	-4.05	405.0	401.4	0.88	399.0	383.0	4.00
2	90	400	250	456.9	448.9	1.75	450.8	457.6	-1.50	427.2	433.8	-1.56
3	90	500	300	511.2	515.0	-0.74	501.8	513.7	-2.37	493.1	484.7	1.71
4	120	300	250	526.9	509.9	3.23	526.4	519.9	1.23	488.1	511.7	-4.84
5	120	400	300	572.9	576.0	-0.54	583.5	576.1	1.27	579.8	562.6	2.97
6	120	500	200	532.9	525.5	1.39	532.2	515.9	3.06	441.8	470.9	-6.59
7	150	300	300	633.7	637.0	-0.52	639.7	638.4	0.19	629.1	640.5	-1.81
8	150	400	200	583.9	586.5	-0.45	555.1	578.3	-4.17	576.3	548.8	4.77
9	150	500	250	647.8	652.6	-0.74	641.3	634.5	1.07	601.3	599.6	0.28

**Table 11.**  
Predicted MRR values of regression model for t = 8 mm.

straight and arc profiles at 4, 8 and 12 mm AISI 304L thicknesses display comparable results. Further, the results reveal that traverse speed and waterjet pressure are statistically and physically significant factors for obtaining *p*-Values < 0.05. Hence, the abrasive mass flow rate features as a low impacting input parameter for obtaining *p*-Values greater than the acceptable value of 0.05, ranging from 0.002 to 0.751.

The percentage contribution of variables for the most fitted regression models MRR for 4, 8 and 12 mm material thicknesses are illustrated in **Figure 6**. In general, traverse speed is indicated as the most impacting variable, followed by waterjet pressure and abrasive mass flow rate, with a percent contribution ranging from 71.14–78.94%, 12.11–24.09% and 2.65–9.03% respectively for all profiles and material thicknesses. It is apparent here that the percentage contribution of traverse speed increases

Exp. no.	Independent variables			MRR 1 (mm <sup>3</sup> /min)			MRR 2 (mm <sup>3</sup> /min)			MRR 3 (mm <sup>3</sup> /min)		
	X <sub>1</sub>	X <sub>2</sub>	X <sub>3</sub>	Exp.	Pred.	Error %	Exp.	Pred.	Error %	Exp.	Pred.	Error %
1	90	300	200	472.0	491.5	-4.13	506.3	523.4	-3.37	528.9	523.1	1.10
2	90	400	250	586.2	576.9	1.58	542.1	569.5	-5.05	588.7	601.5	-2.17
3	90	500	300	655.9	662.4	-0.99	625.7	615.6	1.62	665.4	679.9	-2.18
4	120	300	250	676.0	653.4	3.35	731.7	683.2	6.62	687.5	679.6	1.15
5	120	400	300	735.0	738.8	-0.51	735.8	729.3	0.88	772.3	758.0	1.85
6	120	500	200	701.2	686.7	2.07	712.3	698.7	1.90	695.1	674.4	2.98
7	150	300	300	813.0	815.2	-0.27	822.4	843.1	-2.51	835.4	836.1	-0.09
8	150	400	200	755.6	763.1	-1.00	811.9	812.5	-0.07	725.0	752.5	-3.79
9	150	500	250	841.6	848.6	-0.83	845.6	858.6	-1.54	837.6	830.9	0.80

**Table 12.**  
 Predicted MRR values of regression model for t = 12 mm.

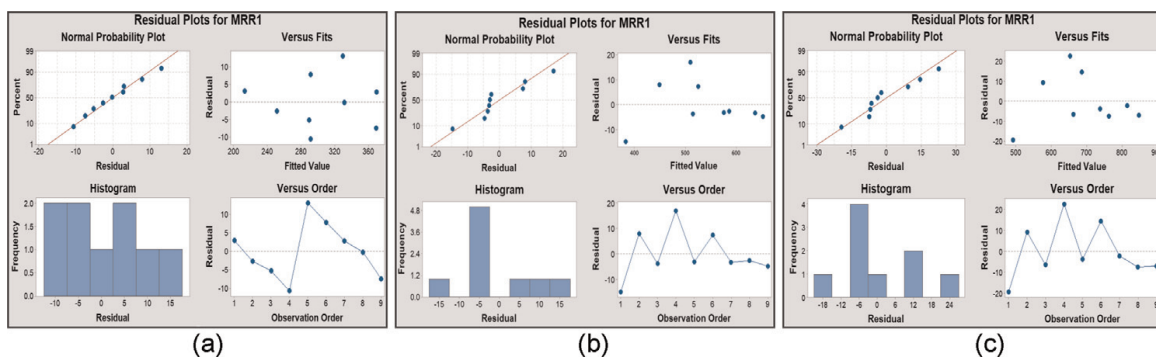


**Figure 6.**  
 Residual plots for material removal rate. (a) MRR 1 (mm<sup>3</sup>/min) for t = 4 mm (b) MRR 1 (mm<sup>3</sup>/min) for t = 8 mm (c) MRR (mm<sup>3</sup>/min) for t = 12 mm.

in range from 71.4 to 77.55% as the material thickness increases. An increasing traverse speed reinforces the contact time of the waterjet with the abrasive on the material, producing a higher volume rate of material to the machine [9]. Contrastingly, the percentage contribution of waterjet pressure and abrasive mass flow rate decreased as the material thickness and traverse speed increased, ranging from 22.42–12.11% and 4.35–9.03%, respectively. The increasing traverse speed and depth or thickness of the material to cut, results in a more prolonged machining process, which gradually leads to subsiding kinetic energy and loss of large of abrasive particles, resulting in reduced effectiveness of abrasive mass flow rate and waterjet pressure during the erosion process (Figure 7) [9, 47].

### 3.3 Regression model and analysis for kerf taper angle

The summary of the multi-linear regression coefficients for kerf taper angle of straight-line, inner and outer arc profiles using 4, 8 and 12 mm material thicknesses are detailed in Table 13. The results provide a similar trend, showing the constant sign

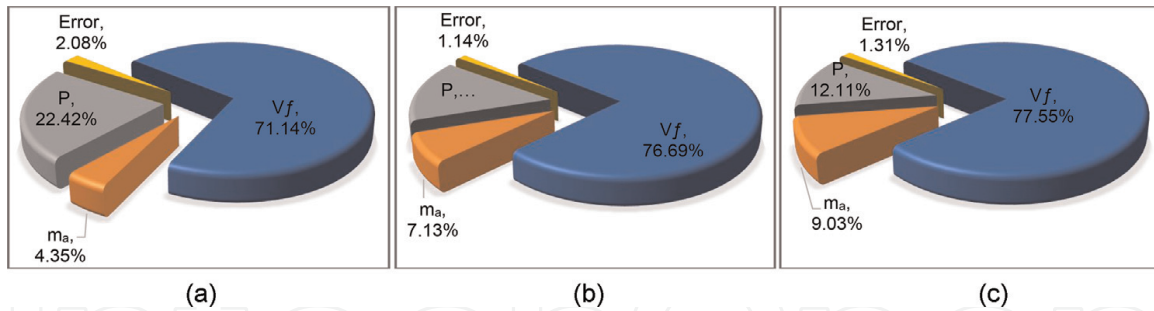


**Figure 7.** Percentage contribution of variables for material removal rate. (a) MRR<sub>1</sub> ( $\text{mm}^3/\text{min}$ ) for  $t = 4$  mm (b) MRR<sub>1</sub> ( $\text{mm}^3/\text{min}$ ) for  $t = 8$  mm (c) MRR ( $\text{mm}^3/\text{min}$ ) for  $t = 12$  mm.

as positive, with variables  $X_1$ ,  $X_2$  and  $X_3$  as negative for all profiles and thicknesses. If the coefficient sign is negative, as the variable increases, the response decreases, whereas if the coefficient is positive, the relationship between variables and responses is directly proportional [44]. Therefore, an increasing rate of traverse speed ( $X_1$ ) results in an increasing angle of the kerf taper. Thus, an increasing rate of abrasive mass flow and waterjet pressure reduces the value of kerf taper angle. The values of  $R^2$ ,  $R^2_{\text{adj}}$  and  $R^2_{\text{pred}}$  for 4, 8 and 12 mm ranged from 94.74–99.37%, 91.59–98.99% and 80.11–97.66%, respectively. This confirms that regression models are reliable in representing correlation between variables and responses and can be used in the optimisation of process parameters.

The coefficient of determination ( $R^2$ ,  $R^2_{\text{adj}}$  and  $R^2_{\text{pred}}$ ) obtained from straight-line, inner and outer arc profiles for all material thicknesses had a similar and consistent gap of at least 2%. The AWJM provides comparable behaviour in processing both straight and curvature profiles [36]. The highest values of  $R^2$ ,  $R^2_{\text{adj}}$  and  $R^2_{\text{pred}}$  for 4 and 8 mm material thicknesses were attained in KTA1 with values of 97.56, 96.09 and 90.57%; 98.02, 96.82 and 92.01%; 99.37, 98.99 and 97.66%, respectively. These are the most fitted model, to be utilised in the optimisation of the process parameters of this study.

The predicted KTA values using the regression models applied for straight-line, inner and outer arc profiles of the three levels of material thicknesses are detailed in **Tables 14-16**. The percentage error obtained for 4, 8 and 12 mm AISI 304L thicknesses ranged between  $-2.55$  to  $1.72\%$ ,  $-2.67$  to  $3.74\%$  and  $-3.14$  to  $2.43\%$ , respectively. The errors calculated for KTA between the predicted value and experimental results were less than the acceptable maximum limit of 20%, indicating the reliability of the models in predicting KTA values.

**Figure 8** illustrates the residual plot for KTA including normal probability plot, residual versus fits, histogram for residuals and residuals versus experimental values. The results showed that the most fitted regression model is achieved from KTA1 for all material thicknesses. Correspondingly, the normal probability plots for all material thicknesses present a near fit to a line in a normal probability graph. The points constructing an approximate straight-line and plotted along the fitted line signifies that the data is normally distributed and there is a good relation between experimental data and predicted values [45]. Predominantly, the residuals versus fits and observation graph for each material thickness exhibit that the points are plotted randomly and near both sides of 0 with no identified pattern denoting a minimal deviation within residuals and estimated values. **Figure 8** also presents the histogram graph for KTA

Term	<i>t</i> = 4 mm			<i>t</i> = 8 mm			<i>t</i> = 12 mm		
	KTA1	KTA2	KTA3	KTA1	KTA2	KTA3	KTA1	KTA2	KTA3
	Coef	Coef	Coef	Coef	Coef	Coef	Coef	Coef	Coef
	0.9674	1.0469	1.064	1.386	1.483	1.544	1.5981	1.971	1.998
$\beta_1$	0.002414	0.002155	0.001501	0.006143	0.003594	0.004333	0.006568	0.004556	0.004736
$\beta_2$	- 0.000235	- 0.000220	- 0.000136	-0.00052	-0.000525	-0.00035	- 0.000107	- 0.000400	- 0.000436
$\beta_3$	- 0.000932	- 0.000952	- 0.000668	-0.002039	-0.001346	- 0.001867	- 0.002319	- 0.002320	- 0.002286
Model Summary									
R <sup>2</sup>	97.56%	97.26%	94.74%	98.02%	94.76%	96.79%	99.37%	96.30%	96.95%
R <sup>2</sup> (adj)	96.09%	95.61%	91.59%	96.82%	91.61%	94.87%	98.99%	94.08%	95.12%
R <sup>2</sup> (pred)	90.57%	88.61%	84.48%	92.01%	80.11%	88.29%	97.66%	86.50%	88.70%

**Table 13.**  
Summary of linear regression coefficients for KTA.

Exp. no.	Independent variables			KTA1 (°)			KTA2 (°)			KTA3 (°)		
	X <sub>1</sub>	X <sub>2</sub>	X <sub>3</sub>	Exp.	Pred.	Error %	Exp.	Pred.	Error %	Exp.	Pred.	Error %
1	90	300	200	0.93	0.93	0.23	0.99	0.98	0.41	1.02	1.02	-0.19
2	90	400	250	0.86	0.86	0.26	0.92	0.92	0.84	0.98	0.98	0.15
3	90	500	300	0.77	0.79	-2.30	0.83	0.85	-2.16	0.94	0.93	0.53
4	120	300	250	0.95	0.95	-0.60	1.00	1.00	0.16	1.04	1.04	0.78
5	120	400	300	0.90	0.88	1.74	0.94	0.93	1.33	0.96	0.99	-2.55
6	120	500	200	0.97	0.95	1.72	1.00	1.01	-0.20	1.05	1.04	0.70
7	150	300	300	0.98	0.98	0.34	1.01	1.02	-0.80	1.06	1.05	1.13
8	150	400	200	1.03	1.05	-1.70	1.08	1.09	-1.44	1.09	1.10	-1.21
9	150	500	250	0.98	0.98	0.09	1.04	1.02	1.68	1.06	1.05	0.54

**Table 14.**  
Predicted KTA values of regression model for t = 4 mm.

Exp. no.	Independent variables			KTA1 (°)			KTA2 (°)			KTA3 (°)		
	X <sub>1</sub>	X <sub>2</sub>	X <sub>3</sub>	Exp.	Pred.	Error %	Exp.	Pred.	Error %	Exp.	Pred.	Error %
1	90	300	200	1.38	1.38	0.04	1.40	1.38	1.42	1.43	1.46	-1.83
2	90	400	250	1.22	1.22	-0.12	1.27	1.26	0.76	1.34	1.33	0.91
3	90	500	300	1.04	1.07	-2.65	1.13	1.14	-0.94	1.21	1.20	0.87
4	120	300	250	1.48	1.46	1.50	1.43	1.42	0.43	1.54	1.49	3.07
5	120	400	300	1.35	1.30	3.42	1.30	1.30	-0.07	1.35	1.36	-1.07
6	120	500	200	1.44	1.46	-0.81	1.34	1.38	-3.20	1.49	1.52	-1.75
7	150	300	300	1.50	1.54	-2.67	1.44	1.46	-1.67	1.50	1.53	-1.96
8	150	400	200	1.68	1.69	-0.61	1.53	1.54	-0.81	1.70	1.68	1.11
9	150	500	250	1.56	1.54	1.41	1.48	1.42	3.74	1.56	1.55	0.46

**Table 15.**  
Predicted KTA values of regression model for t = 8 mm.

illustrating the distribution or frequency of the residuals for all observations. The results show that the frequency of KTA for 4, 8 and 12 mm material thicknesses range from -0.002 to 0.015, -0.05 to 0.05 for 8 mm and -0.02 to 0.03, respectively. These graphs reveal a minimal interval or inequalities of the experimental data indicating that the KTA regression models are highly fitted to concrete prediction [46].

**Tables A7-A9** in the Appendix section detail the results of ANOVA, where it can be observed that the impacts of parameters for all profiles and three levels of material thicknesses demonstrate a similar trend, denoting traverse speed and waterjet pressure to be significant factors for acquiring *p*-Values lower than 0.05. Thus, the abrasive mass flow rate was found insignificant for achieving *p*-Values >0.05, ranging from 0.002 to 0.245 for all profiles and material thicknesses.

Exp. no.	Independent variables			KTA1 (°)			KTA2 (°)			KTA3 (°)		
	X <sub>1</sub>	X <sub>2</sub>	X <sub>3</sub>	Exp.	Pred.	Error %	Exp.	Pred.	Error %	Exp.	Pred.	Error %
1	90	300	200	1.70	1.69	0.39	1.80	1.80	0.18	1.85	1.84	0.49
2	90	400	250	1.57	1.57	0.07	1.63	1.64	-0.48	1.67	1.68	-0.26
3	90	500	300	1.43	1.44	-0.70	1.45	1.49	-2.20	1.49	1.52	-2.08
4	120	300	250	1.79	1.77	0.87	1.83	1.82	0.92	1.88	1.86	0.88
5	120	400	300	1.65	1.65	0.14	1.67	1.66	0.60	1.71	1.71	0.43
6	120	500	200	1.86	1.87	-0.72	1.90	1.85	2.43	1.92	1.89	1.51
7	150	300	300	1.84	1.86	-0.85	1.85	1.84	0.52	1.89	1.89	0.13
8	150	400	200	2.06	2.08	-0.81	1.97	2.03	-3.14	2.02	2.08	-2.93
9	150	500	250	1.98	1.95	1.51	1.89	1.87	0.82	1.95	1.92	1.55

**Table 16.**  
 Predicted KTA values of regression model for  $t = 12$  mm.

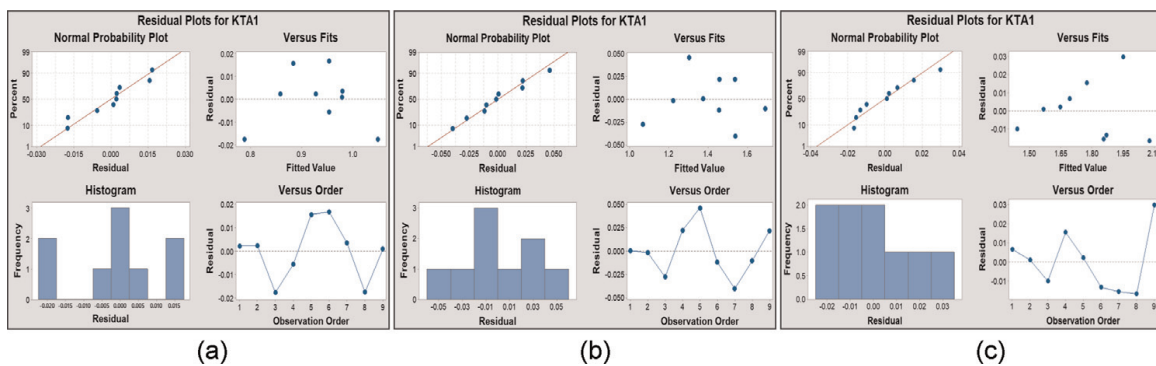


**Figure 8.**  
 Residual plots for kerf taper angle. (a) KTA<sub>1</sub> (°) for  $t = 4$  mm (b) KTA<sub>1</sub> (°) for  $t = 8$  mm (c) KTA<sub>1</sub> (°) for  $t = 12$  mm.

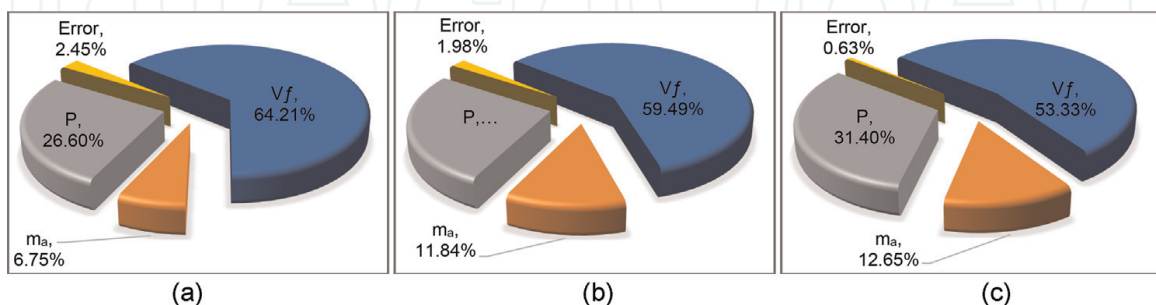


**Figure 9.**  
 Percentage contribution of variables for kerf taper angle. (a)  $t = 4$  mm (b)  $t = 8$  mm (c)  $t = 12$  mm.

**Figure 9** exhibits the percentage contribution of variables for KTA for the most fitted regression models for 4, 8 and 12 mm material thickness. Traverse speed was the most influencing parameter, followed by waterjet pressure and abrasive mass flow rate, in agreement with previous studies [14, 37]. The obtained

results have shown that the influence of traverse speed decreases in range from 64.21 to 53.33% as the material thickness increases. An increasing value traverse speed results in the loss of a large number of abrasive particles, continuously dropping as the material thickness also increases, leading to a higher angle of kerf taper [50]. **Figure 9** shows increases of material thickness, the percentage contribution of waterjet pressure and abrasive mass flow rate, ranging from 26.60 to 33.40% and 6.75 to 12.65%, respectively. This increasing value of waterjet pressure resulted in higher energy, generating a larger amount of abrasive particles that result in a lower kerf taper [51]. Moreover, a rising rate of abrasive mass flow breaks down abrasive particles into a smaller scale, generating more sharp points that results in reduction of kerf taper angle [51].

#### 4. Response surface methodology multi-objective optimisation

In this research, multi-objective optimisation was performed using RSM to determine the optimum process parameters of abrasive waterjet contour cutting of AISI 304L with varied thicknesses using MINITAB 19 software. The following optimisation objectives were stated as follows:

$$f_1 = \text{Min} (R_a) \quad (8)$$

$$f_2 = \text{Min} (KTA) \quad (9)$$

$$f_3 = \text{Max} (MRR) \quad (10)$$

RSM optimisation was performed using the models with the highest determination of coefficients, i.e.,  $R^2$ ,  $R^2_{\text{adj}}$  and  $R^2_{\text{pred}}$ . Accordingly, the regression models utilised to minimise surface roughness were  $R_{a3}$  for 4 and 8 mm and  $R_{a2}$  for 12 mm.  $MRR_1$  and  $KTA_1$  models were used for all material thicknesses.

The Regression models utilised in multi-objective optimisation for varied thicknesses of AISI 304L were expressed by Eqs. (8)-(16).

$$Ra_{4\text{mm}} = 1.4256 + 0.003222 X_1 - 0.000217 X_2 - 0.001133 X_3 \quad (11)$$

$$KTA_{4\text{mm}} = 0.9674 + 0.002414 X_1 - 0.000235 X_2 - 0.000932 X_3 \quad (12)$$

$$MRR_{4\text{mm}} = -84.2 + 1.752 X_1 + 0.126 X_2 + 0.5103 X_3 \quad (13)$$

$$Ra_{8\text{mm}} = 1.76 + 0.008869 X_1 - 0.000577 X_2 - 0.001920 X_3 \quad (14)$$

$$KTA_{8\text{mm}} = 1.386 + 0.006143 X_1 - 0.000520 X_2 - 0.002039 X_3 \quad (15)$$

$$MRR_{8\text{mm}} = -119 + 2.941X_1 + 0.2723 X_2 + 0.777X_3 \quad (16)$$

$$Ra_{4\text{mm}} = 2.3854 + 0.004276 X_1 - 0.000446 X_2 - 0.001924 X_3 \quad (17)$$

$$KTA_{4\text{mm}} = 1.5981 + 0.006568 X_1 - 0.000107 X_2 - 0.002319 X_3 \quad (18)$$

$$MRR_{8\text{mm}} = -158.8 + 3.867X_1 + 0.396 X_2 + 0.917 X_3 \quad (19)$$

In simultaneous optimisation, goals and boundaries must be defined for each process parameter. Targets are based on the experimental data obtained, referring to the set highest value of responses for maximising MRR and lowest value of responses for minimising  $R_a$  and KTA. In this optimisation, process parameters and defined objectives were assigned to be equally significant. Therefore, the equal weights

(wt. = 1) were assigned in order to achieve an equal importance to the process parameters and objectives. The constraints referring to range and limits of the process parameters are detailed below.

Constraints:

$$90 \leq V_f \leq 150 \text{ mm/min}$$

$$300 \leq m_a \leq 500 \text{ g/min}$$

$$200 \leq P \leq 300 \text{ g/min}$$

Limits:

$$KTA_{4\text{mm}} \leq 1.03^\circ, KTA_{8\text{mm}} \leq 1.68^\circ, KTA_{12\text{mm}} \leq 2.06^\circ$$

$$Ra_{4\text{mm}} \text{ mm} 1.58 \mu\text{m}, Ra_{8\text{mm}} \text{ mm} 2.45 \mu\text{m}, Ra_{12\text{mm}} \text{ mm} 2.46 \mu\text{m}$$

$$MRR_{4\text{mm}} \geq 216.20 \text{ mm}^3/\text{min}, MRR_{8\text{mm}} \geq 367.90 \text{ mm}^3/\text{min},$$

$$MRR_{12\text{mm}} \geq 472.00 \text{ mm}^3/\text{min}$$

**Table 17** shows the solutions for multi-objective optimisation performed for 4, 8 and 12 mm thickness of AISI 304L. The solution that provides the value of composite desirability nearest to 1 can be considered as the best solution [40]. **Table 17** reveals that solution 1 is the best for 4, 8 and 12 mm material thicknesses, achieving composite desirability values of 0.748448, 0.780587 and 0.786800, respectively. There are three solutions generated from MINITAB application, providing the settings of input variables, achieved values of responses and composite desirability. Solution 1 provides the optimum settings of input parameters i.e.,  $V_f$  for 4, 8 and 12 mm material thicknesses, at the speeds of 95, 90 and 91 mm/min, respectively. The obtained optimum setting for  $m_a$  and  $P$  were found to be the same value for all material thicknesses, at 500 g/min and 200 MPa, respectively. **Table 17** presents the minimum achieved values of KTA and  $R_a$  and maximum MRR for 4, 8 and 12 mm material thicknesses, featuring at  $0.799^0$ ,  $1.283 \mu\text{m}$  and  $297.98 \text{ mm}^3/\text{min}$ ;  $1.068^0$ ,  $1.694 \mu\text{m}$  and  $514.97 \text{ mm}^3/\text{min}$  and  $1.448^0$ ,  $1.975 \mu\text{m}$  and  $667.07 \text{ mm}^3/\text{min}$ , respectively.

An optimisation plot presenting how the variables affected the predicted responses is shown in **Figure 10**, detailing the composite desirability for multi-objective (D) and single-objective optimisation (d). Current variable settings for the input parameters are presented in the figure, alongside with lower and upper limits. **Figure 10** shows a three-sectioned line graph representing the correlation of KTA,  $R_a$  and MRR against traverse speed ( $X_1$ ), abrasive mass flow rate ( $X_2$ ) and waterjet pressure ( $X_3$ ).

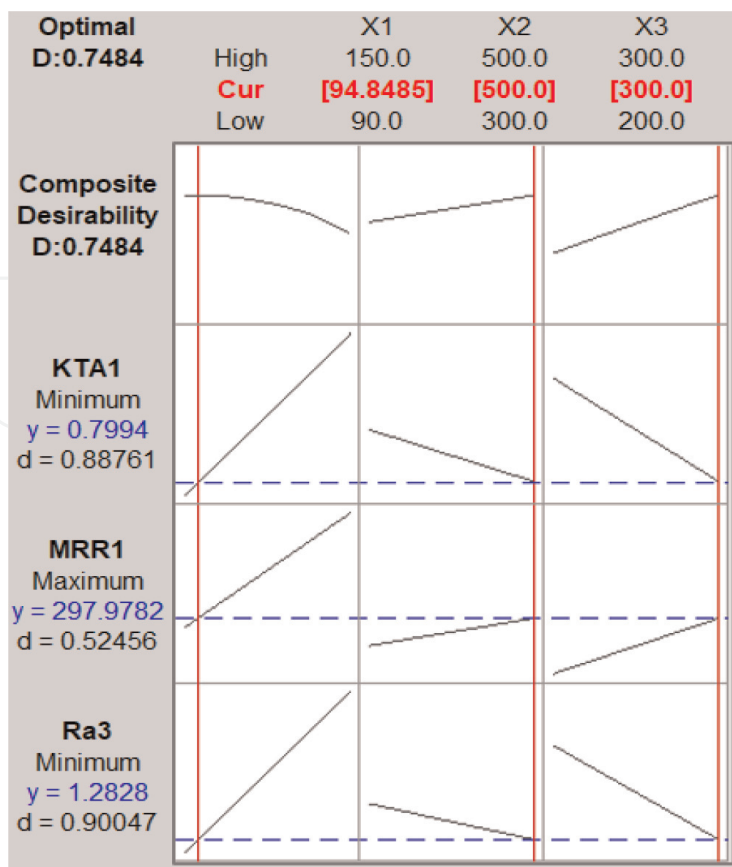
From the figure, it can be observed that abrasive waterjet contour cutting responses demonstrate a comparable behaviour against input parameters for all material thicknesses. The highest rate of material removal and lowest value of surface roughness and Kerf taper angle were achieved by employing a rate of 150 mm/min speed, 500 g/min abrasive mass flow rate, and 300 MPa of waterjet pressure. Increasing water pressure, alongside high velocity abrasive mass flow rate, produces a greater collision of abrasive particles, generating higher rate of material removal and reducing surface roughness and kerf taper angle [52].

The surface roughness displayed an incrementing value that ranged from 4–13% as the rate of traverse speed increased from 90 to 150 mm/min. As the speed increases per unit of area over time, the kinetic energy containing abrasives gradually decreases, resulting in greater evidences of rough surfaces [52]. Consequently, RSM optimisation

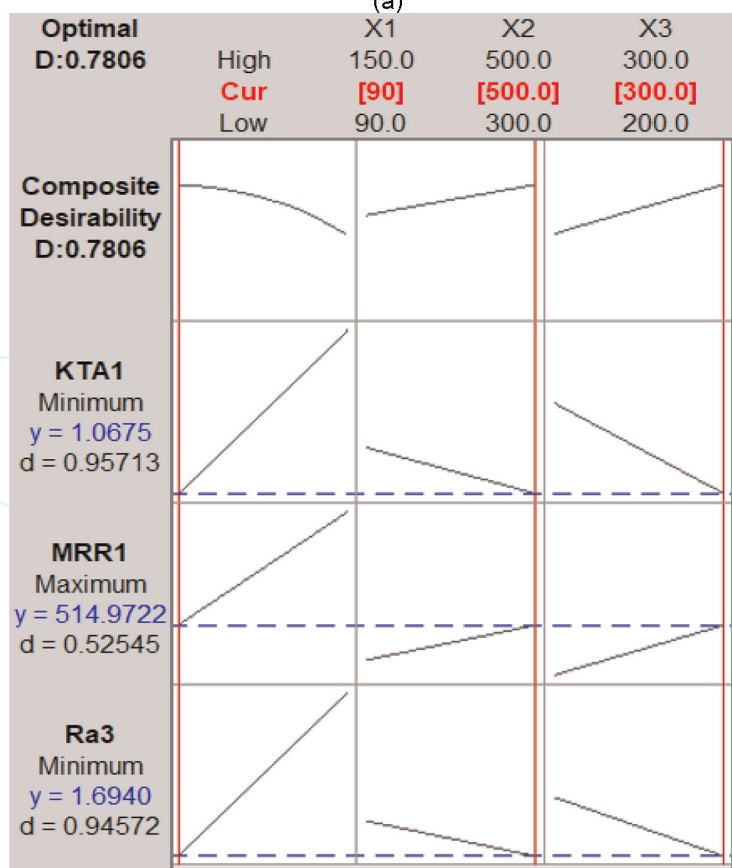


Parameters	4 mm			8 mm			12 mm		
	Solutions								
	1	2	3	1	2	3	1	2	3
$X_1 = V_f$ (mm/min)	95	97	97	90	90	116	91	90	90
$X_2 = m_a$ (g/min)	500	500	500	500	500	301.737	500	500	500
$X_3 = P$ (MPa)	300	300	300	300	300	300	300	300	300
KTA (°)	0.799	0.805	0.805	1.068	1.068	1.330	1.448	1.441	1.441
MRR (mm <sup>3</sup> /min)	297.98	302.17	302.17	514.97	514.97	537.49	667.07	662.78	662.78
R <sub>a</sub> (μm)	1.283	1.291	1.291	1.694	1.694	2.039	1.975	1.970	1.970
Composite Desirability	0.748448	0.748075	0.748075	0.780587	0.780587	0.556566	0.786800	0.786677	0.786677

**Table 17.**  
Solutions for RSM multi-objective optimisation.



(a)



(b)

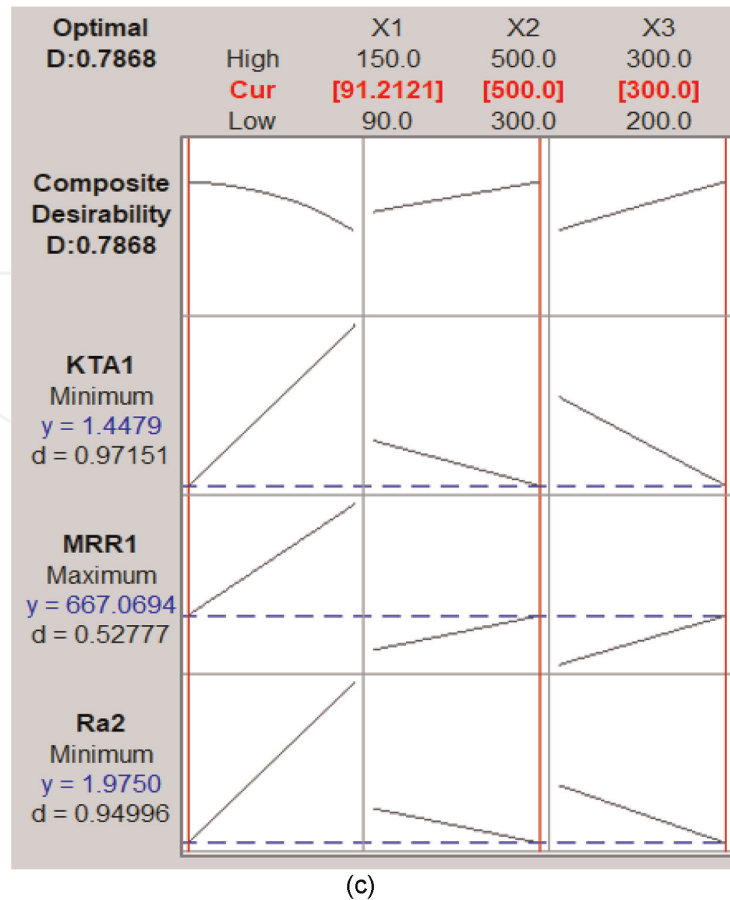


**Figure 10.** Response optimisation plot. (a)  $t = 4$  mm (b)  $t = 8$  mm (c)  $t = 12$  mm.

has shown that a lower level of traverse speed can produce a better quality of cut surface. Additionally, surface roughness in this study shows an increasing value ranging 2–5%, as the waterjet pressure increases and the abrasive mass flow rate from 200 to 300 MPa and 300 to 500 g/min, respectively. In this study, it is confirmed that augmenting abrasive flow rate and waterjet pressure, up to a specific range, lowers the value of surface roughness. When higher values of traverse speed are employed, the material removal exhibits an increasing rate that ranges from 16–20%. In addition, increasing rate of material removal was achieved with a range of 5–9%, as the rate of abrasive mass flow and waterjet pressure increased from 200 to 300 MPa and 300 to 500 g/min, respectively. AWJM produces a high level of kinetic energy, driving a higher level of speed and waterjet pressure alongside with abrasive mass flow rate, which in turn generates higher cutting area per unit of time and generates a larger amount of eroded material [53]. Therefore, the rate of material removal is directly proportional to traverse speed, abrasive mass flow rate and waterjet pressure.

**Figure 10** shows that kerf taper angle values increase as the rate of traverse speed increases from 90 to 150 mm/min. With continuous reduction in the number of abrasive particles, as the traverse speed increases, the cohesion on metal material decreases, generating a higher tapering angle [52]. The kerf taper angle in this study was reduced by 2–7%, as the abrasive mass flow and waterjet pressure were increased from 200 to 300 MPa and 300 to 500 g/min, respectively. A higher waterjet pressure alongside with abrasive mass flow rate reinforces the collision of abrasive particles on the target material, causing the reduction of kerf taper angle [51].

## 5. Conclusions

This study focuses on modelling and establishing optimum abrasive waterjet contour cutting parameters that lead to minimum surface roughness, kerf taper angle and maximum productivity (material removal rate). On the basis of the results achieved and discussed, the following conclusions are accomplished:

1. The experimental results indicate that abrasive waterjet contour cutting responses demonstrate similar behaviour against input parameters for straight-line and curvature profiles. The correlation coefficients of the predictive models of  $R^2$ ,  $R^2_{adj}$  and  $R^2_{pred}$  for surface roughness, kerf taper angle and material removal rate were found to be in the range of 88.66–99.08%, 82.3–98.86% and 82.3–98.86% respectively. Therefore, the developed multi-linear regression models are reliable and effective for predicting output responses, where the percentage errors are at minimum values ranging from –6.59 to 6.71%
2. The results of the ANOVA for  $R_a$ , MRR and KTA demonstrate that traverse speed is the most influencing factor, with percentage contributions ranging from 55.67 to 78.94%. Surface roughness and kerf taper angle decrease as waterjet pressure and abrasive mass flow rate increase, resulting in reductions ranging from 2–5% and 2–7%, respectively. Increasing values of traverse speed, waterjet pressure and abrasive mass flow rate lead to increased rates of material removal, ranging from 16–20% and 5–9%, respectively.
3. The multi-objective optimization was performed using RSM for optimising abrasive waterjet contour cutting process parameters applied for 4, 8 and 12 mm material thicknesses, achieving the highest composite desirability values of 0.748448, 0.780587 and 0.786800, respectively. The optimum settings of input parameters i.e.,  $V_f$  for 4, 8 and 12 mm material thickness are 95, 90 and 91 mm/min, respectively. The obtained optimum settings for  $m_a$  and  $P$  were found to be the same value for all material thicknesses, at 500 g/min and 200 MPa, respectively. The minimum achieved values of KTA and  $R_a$  and maximum MRR for 4, 8 and 12 mm material thickness were  $0.799^0$ ,  $1.283 \mu\text{m}$  and  $297.98 \text{ mm}^3/\text{min}$ ;  $1.068^0$ ,  $1.694 \mu\text{m}$  and  $514.97 \text{ mm}^3/\text{min}$ ; and  $1.448^0$ ,  $1.975 \mu\text{m}$  and  $667.07 \text{ mm}^3/\text{min}$ , respectively.

## Abbreviations and nomenclature

$ht$	depth of cut (mm)
$m_a$	abrasive mass flow rate (g/min)
$P$	water pressure (MPa)
$R_a$	surface roughness ( $\mu\text{m}$ )
$V_f$	traverse speed (mm/min)
$W$	kerf width (mm)
$W_t$	kerf top width (mm)
$W_b$	kerf bottom width (mm)
$t$	thickness of the material (mm)
AISI	austenitic stainless steel
ANOVA	analysis of variance

AWJM      abrasive waterjet machining  
 KTA        kerf taper angle ( $^{\circ}$ )  
 MRR        material removal rate ( $\text{mm}^3/\text{min}$ )

**A. Appendix**

Source	R <sub>a</sub> 1		R <sub>a</sub> 2		R <sub>a</sub> 3	
	Contribution %	p-Value	Contribution %	p-Value	Contribution %	p-Value
X <sub>1</sub>	59.90	0.001	69.43	0.000	69.39	0.000
X <sub>2</sub>	5.16	0.067	3.49	0.068	3.77	0.017
X <sub>3</sub>	30.19	0.002	23.86	0.002	24.09	0.001
Error	4.74		3.23		2.74	
Total	100.00		100		100	

**Table A1.**  
 ANOVA of R<sub>a</sub> for t = 4 mm.

Source	R <sub>a</sub> 1		R <sub>a</sub> 2		R <sub>a</sub> 3	
	Contribution %	p-Value	Contribution %	p-Value	Contribution %	p-Value
X <sub>1</sub>	72.21	0.000	71.07	0.000	64.06	0.000
X <sub>2</sub>	7.96	0.007	11.57	0.003	3.94	0.013
X <sub>3</sub>	17.84	0.001	15.52	0.001	30.64	0.001
Error	1.99		1.84		1.36	
Total	100.00		100.00		100.00	

**Table A2.**  
 ANOVA of R<sub>a</sub> for t = 8 mm.

Source	R <sub>a</sub> 1		R <sub>a</sub> 2		R <sub>a</sub> 3	
	Contribution %	p-Value	Contribution %	p-Value	Contribution %	p-Value
X <sub>1</sub>	57.23	0.000	58.85	0.000	57.21	0.001
X <sub>2</sub>	3.44	0.026	5.31	0.002	17.66	0.011
X <sub>3</sub>	34.59	0.000	33.1	0.000	19.47	0.009
Error	4.74		2.74		3.23	3.23
Total	100.00		100.00		100.00	

**Table A3.**  
 ANOVA of R<sub>a</sub> for t = 12 mm.

Source	MRR 1		MRR 2		MRR 3	
	Contribution %	<i>p</i> -Value	Contribution %	<i>p</i> -Value	Contribution %	<i>p</i> -Value
X <sub>1</sub>	71.14	0.000	70.98	0	75.503	0
X <sub>2</sub>	4.35	0.023	2.65	0.067	3.345	0.048
X <sub>3</sub>	22.42	0.002	23.93	0.001	18.688	0.002
Error	2.08		2.44		2.464	
Total	100.00		100.00		100.00	

**Table A4.**  
ANOVA of MRR for t = 4 mm.

Source	MRR 1		MRR 2		MRR 3	
	Contribution %	<i>p</i> -Value	Contribution %	<i>p</i> -Value	Contribution %	<i>p</i> -Value
X <sub>1</sub>	76.69	0.000	76.12	0.000	70.51	0.000
X <sub>2</sub>	7.13	0.002	3.62	0.038	0.12	0.751
X <sub>3</sub>	15.05	0.000	17.98	0.002	24.09	0.005
Error	1.14		2.29		5.27	
Total	100.00		100.00		100.00	

**Table A5.**  
ANOVA of MRR for t = 8 mm.

Source	MRR 1		MRR 2		MRR 3	
	Contribution %	<i>p</i> -Value	Contribution %	<i>p</i> -Value	Contribution %	<i>p</i> -Value
X <sub>1</sub>	77.55	0.000	78.94	0.000	73.29	0.000
X <sub>2</sub>	9.03	0.002	4.13	0.04	4.15	0.028
X <sub>3</sub>	12.11	0.001	13.3	0.001	20.35	0.001
Error	1.31		3.63		2.21	
Total	100.00		100.00		100.00	

**Table A6.**  
ANOVA of MRR for t = 12 mm.

Source	KTA 1		KTA 2		KTA 3	
	Contribution %	<i>p</i> -Value	Contribution %	<i>p</i> -Value	Contribution %	<i>p</i> -Value
X <sub>1</sub>	64.21	0.000	58.7	0.000	56.74	0.000
X <sub>2</sub>	6.75	0.014	6.77	0.017	5.27	0.075
X <sub>3</sub>	26.6	0.001	31.78	0.001	32.74	0.001
Error	2.45		2.74		5.26	
Total	100.00		100.00		100.00	

**Table A7.**  
ANOVA of KTA for t = 4 mm.

Source	KTA 1		KTA 2		KTA 3	
	Contribution %	<i>p</i> -Value	Contribution %	<i>p</i> -Value	Contribution %	<i>p</i> -Value
X <sub>1</sub>	59.49	0.001	67.49	0.000	60.95	0.000
X <sub>2</sub>	11.84	0.015	5.63	0.013	4.42	0.047
X <sub>3</sub>	26.69	0.002	21.65	0.001	31.42	0.001
Error	1.98		5.24		3.21	
Total	100.00		100.00		100.00	

**Table A8.**  
ANOVA of KTA for  $t = 8$  mm.

Source	KTA 1		KTA 2		KTA 3	
	Contribution %	<i>p</i> -Value	Contribution %	<i>p</i> -Value	Contribution %	<i>p</i> -Value
X <sub>1</sub>	53.33	0.000	70.59	0.000	55.67	0.000
X <sub>2</sub>	12.65	0.055	0.22	0.245	5.24	0.033
X <sub>3</sub>	31.40	0.001	25.50	0.000	36.04	0.001
Error	0.63		3.70		3.05	
Total	100.00		100.00		100.00	


**Table A9.**  
ANOVA of KTA for  $t = 12$  mm.

## Author details

Jennifer Milaor Llanto, Ana Vafadar and Majid Tolouei-Rad\*  
School of Engineering, Edith Cowan University, Joondalup, Australia

\*Address all correspondence to: m.rad@ecu.edu.au

## IntechOpen

© 2022 The Author(s). Licensee IntechOpen. This chapter is distributed under the terms of the Creative Commons Attribution License (<http://creativecommons.org/licenses/by/3.0>), which permits unrestricted use, distribution, and reproduction in any medium, provided the original work is properly cited. 

## References

- [1] Radovanović M. Multi-objective optimization of process performances when cutting carbon steel with abrasive water jet. *Tribology in Industry*. 2016;**38**(4):1741-1759
- [2] Liu X et al. Waterjet machining and research developments: A review. *The International Journal of Advanced Manufacturing Technology*. 2019; **102**(5):1257-1335
- [3] Rajurkar K et al. Review of sustainability issues in non-traditional machining processes. *Procedia Manufacturing*. 2017;**7**:714-720
- [4] Natarajan Y et al. Abrasive water jet machining process: A state of art of review. *Journal of Manufacturing Processes*. 2020;**49**:271-322
- [5] Singh P et al. Developments of non-conventional drilling methods—a review. *The International Journal of Advanced Manufacturing Technology*. 2020;**106**(5):2133-2166
- [6] Sureban R, Kulkarni VN, Gaitonde V. Modern optimization techniques for advanced machining processes—a review. *Materials Today: Proceedings*. 2019;**18**:3034-3042
- [7] Rao RV, Rai DP, Balic J. Optimization of abrasive waterjet machining process using multi-objective jaya algorithm. *Materials Today-Proceedings*. 2018;**5**(2): 4930-4938
- [8] Nair A, Kumanan S. Multi-performance optimization of abrasive water jet machining of Inconel 617 using WPCA. *Materials and Manufacturing Processes*. 2017;**32**(6):693-699
- [9] Chakraborty S, Mitra A. Parametric optimization of abrasive water-jet machining processes using grey wolf optimizer. *Materials and Manufacturing Processes*. 2018;**33**(13):1471-1482
- [10] Trivedi P, Dhanawade A, Kumar S. An experimental investigation on cutting performance of abrasive water jet machining of austenite steel (AISI 316L). *Advances in Materials and Processing Technologies*. 2015;**1**(3–4):263-274
- [11] Gnanavelbabu A et al. Experimental investigations on multiple responses in abrasive waterjet machining of Ti-6Al-4V alloy. *Materials Today: Proceedings*. 2018;**5**(5):13413-13421
- [12] Jeykrishnan J et al. Optimization of process parameters in abrasive water jet machining/cutting (AWJM) of nickel alloy using traditional analysis to minimize kerf taper angle. *Materials Today: Proceedings*. 2019;**16**:392-397
- [13] Singh D, Shukla RS. Investigation of kerf characteristics in abrasive water jet machining of inconel 600 using response surface methodology. *Defence Science Journal*. 2020;**70**(3):313-322
- [14] Madankar A et al. Estimation and control of surface quality and traverse speed in abrasive water jet machining of AISI 1030 steel using different work-piece thicknesses by RSM. *Australian Journal of Mechanical Engineering*. 2021: **1**:1-8
- [15] Llanto JM et al. Recent progress trend on abrasive waterjet cutting of metallic materials: A review. *Applied Sciences*. 2021;**11**(8):3344
- [16] Pérez L, Carmelo J. On the application of a design of experiments along with an anfis and a desirability function to model response variables. *Symmetry*. 2021;**13**(5):897



- [17] Luis Pérez C. A proposal of an adaptive neuro-fuzzy inference system for modeling experimental data in manufacturing engineering. *Mathematics*. 2020;**8**(9):1390
- [18] Jiang W et al. Effects of nanostructural hierarchy on the hardness and thermal stability of an austenitic stainless steel. *Journal of Materials Research and Technology*. 2021;**12**: 376-384
- [19] Ramana MV et al. Optimization and influence of process parameters of dissimilar SS304L–SS430 joints produced by Robotic TIG welding. *Materials Today: Proceedings*. 2020;**23**: 479-482
- [20] Doreswamy D et al. Machining of d2 heat treated steel using abrasive water jet: The effect of standoff distance and feed rate on kerf width and surface roughness. *International Journal of Research in Engineering and Technology*. 2014;**3**(8):417-421
- [21] Shibin R et al. Investigation on the abrasive water jet machinability of AA2014 using SiC as abrasive. *Materials Today: Proceedings*. 2020;**21**:519-522
- [22] Radovanovic M, Herghelegiu E. Perpendicularity deviation and surface roughness in abrasive water jet cutting of carbon steel. *Revista de Tehnologii Neconventionale*. 2016;**20**(2):39
- [23] Maneiah D et al. Optimization of machining parameters for surface roughness during abrasive water jet machining of aluminium/magnesium hybrid metal matrix composites. *Materials Today: Proceedings*. 2020;**27**: 1293-1298
- [24] Rajamanickam S et al. Comparative analysis of MRR on abrasive water jet machining parameters over aerospace alloys: Inconel 825 & Ti-6Al-4V. *International Journal of Pure and Applied Mathematics*. 2018;**118**:727-733
- [25] Kaladhar M, Subbaiah KV, Rao CS. Machining of austenitic stainless steels—a review. *International Journal of Machining and Machinability of Materials*. 2012;**12**(1):178-192
- [26] Hlaváč LM et al. Investigation of the taper of kerfs cut in steels by AWJ. *The International Journal of Advanced Manufacturing Technology*. 2015; 77(9–12):1811-1818
- [27] Pawar PJ, Vidhate US, Khalkar MY. Improving the quality characteristics of abrasive water jet machining of marble material using multi-objective artificial bee colony algorithm. *Journal of Computational Design and Engineering*. 2018;**5**(3):319-328
- [28] Hlaváč LM et al. Shape distortion reduction method for abrasive water jet (AWJ) cutting. *Precision Engineering*. 2018;**53**:194-202
- [29] Aamir M et al. Optimization and modeling of process parameters in multi-hole simultaneous drilling using taguchi method and fuzzy logic approach. *Materials*. 2020;**13**(3):680
- [30] Msomi V, Mabuwa S. Analysis of material positioning towards microstructure of the friction stir processed AA1050/AA6082 dissimilar joint. *Advances in Industrial and Manufacturing Engineering*. 2020;**1**: 100002
- [31] Lin C. Use of the Taguchi method and grey relational analysis to optimize turning operations with multiple performance characteristics. *Materials and Manufacturing Processes*. 2004; **19**(2):209-220

- [32] Aamir M et al. Feasibility of tool configuration and the effect of tool material, and tool geometry in multi-hole simultaneous drilling of Al2024. *The International Journal of Advanced Manufacturing Technology*. 2020;**111**(3): 861-879
- [33] Nagaraj Y et al. Prediction of material removal rate and surface roughness in hot air assisted hybrid machining on soda-lime-silica glass using regression analysis and artificial neural network. *Silicon*. 2020;**13**(11):1-13
- [34] Aydin G, Karakurt I, Hamzacebi C. Artificial neural network and regression models for performance prediction of abrasive waterjet in rock cutting. *The International Journal of Advanced Manufacturing Technology*. 2014;**75**(9-12):1321-1330
- [35] Cetin MH et al. Evaluation of vegetable based cutting fluids with extreme pressure and cutting parameters in turning of AISI 304L by Taguchi method. *Journal of Cleaner Production*. 2011;**19**(17-18):2049-2056
- [36] Llanto JM et al. Analysis and optimization of process parameters in abrasive waterjet contour cutting of AISI 304L. *Metals*. 2021;**11**(9):1362
- [37] Llanto JM et al. Impacts of traverse speed and material thickness on abrasive waterjet contour cutting of austenitic stainless steel AISI 304L. *Applied Sciences*. 2021;**11**(11):4925
- [38] Aamir M et al. Machinability of Al2024, Al6061, and Al5083 alloys using multi-hole simultaneous drilling approach. *Journal of Materials Research and Technology*. 2020;**9**(5):10991-11002
- [39] Koli Y, Yuvaraj N, Aravindan S. Multi-response mathematical model for optimization of process parameters in CMT welding of dissimilar thickness AA6061-T6 and AA6082-T6 alloys using RSM-GRA coupled with PCA. *Advances in Industrial and Manufacturing Engineering*. 2021;**2**:100050
- [40] Kumar KR, Sreebalaji V, Pridhar T. Characterization and optimization of abrasive water jet machining parameters of aluminium/tungsten carbide composites. *Measurement*. 2018;**117**: 57-66
- [41] Chabbi A et al. Predictive modeling and multi-response optimization of technological parameters in turning of polyoxymethylene polymer (POM C) using RSM and desirability function. *Measurement*. 2017;**95**:99-115
- [42] Chate GR et al. Study of the effect of nano-silica particles on resin-bonded moulding sand properties and quality of casting. *Silicon*. 2018;**10**(5):1921-1936
- [43] Javed SA et al. A critical review: Shape optimization of welded plate heat exchangers based on grey correlation theory. *Applied Thermal Engineering*. 2018;**144**:593-599
- [44] Ratner B. The correlation coefficient: Its values range between + 1/ - 1, or do they? *Journal of Targeting, Measurement and Analysis for Marketing*. 2009;**17**(2):139-142
- [45] Deshpande Y, Andhare A, Sahu NK. Estimation of surface roughness using cutting parameters, force, sound, and vibration in turning of Inconel 718. *Journal of the Brazilian Society of Mechanical Sciences and Engineering*. 2017;**39**(12):5087-5096
- [46] Galpin JS, Hawkins DM. The use of recursive residuals in checking model fit in linear regression. *The American Statistician*. 1984;**38**(2):94-105

[47] Sasikumar K et al. A study on kerf characteristics of hybrid aluminium 7075 metal matrix composites machined using abrasive water jet machining technology. *Proceedings of the Institution of Mechanical Engineers, Part B: Journal of Engineering Manufacture*. 2018;**232**(4): 690-704

[48] Kechagias J, Petropoulos G, Vaxevanidis N. Application of Taguchi design for quality characterization of abrasive water jet machining of TRIP sheet steels. *The International Journal of Advanced Manufacturing Technology*. 2012;**62**(5–8):635-643

[49] Andrzej P. Experimental research into alternative abrasive material for the abrasive water-jet cutting of titanium. *The International Journal of Advanced Manufacturing Technology*. 2018;**97**(1–4):1529-1540

[50] Uthayakumar M et al. Machinability of nickel-based superalloy by abrasive water jet machining. *Materials and Manufacturing Processes*. 2016;**31**(13): 1733-1739

[51] Babu MN, Muthukrishnan N. Exploration on Kerf-angle and surface roughness in abrasive waterjet machining using response surface method. *Journal of The Institution of Engineers (India): Series C*. 2018;**99**(6): 645-656

[52] Ishfaq K et al. Abrasive waterjet cutting of clad material: Kerf taper and MRR analysis. *Materials and Manufacturing Processes*. 2019;**34**(5): 544-553

[53] Kmec J et al. The predictive model of surface texture generated by abrasive water jet for austenitic steels. *Applied Sciences*. 2020;**10**(9):3159